

©Copyright 2016

Yaoyu Yang

Design, Construction, and Validation
of Dynamic Gene Circuits in Yeast

Yaoyu Yang

A dissertation
submitted in partial fulfillment of the
requirements for

Doctor of Philosophy

University of Washington

2016

Reading Committee::

Eric Klavins, Chair

Georg Seelig

Jennifer L Nemhauser

Program Authorized to Offer Degree:
Electrical Engineering

University of Washington

Abstract

Design, Construction, and Validation of Dynamic Gene Circuits in Yeast

Yaoyu Yang

Chair of the Supervisory Committee:
Professor Eric Klavins
Department of Electrical Engineering

Cells are dynamical systems that constantly change and evolve following underlying rules governed by their genetic programs and interactions with a changing environment. Gene circuits that exhibit dynamic behavior, such as bistable switches and oscillators, are designed, constructed, and validated in synthetic biology with the aim of understanding the dynamics of biological systems and gaining the ability to engineer them. However, it remains challenging to construct even the most basic dynamic gene circuits such as bistable switch or oscillator in yeast, the model eukaryote that is of great interest to synthetic biology. Most academic labs use the typical design, build, and test cycle to build dynamic gene circuits, but the build and test components are often old fashioned, highly reliant on expert knowledge, error-prone, low-throughput, and difficult to debug. These challenges greatly hinder progress in engineering dynamic gene circuits. In this thesis, we present the design, analysis, and results of engineering dynamic gene circuits in the yeast *Saccharomyces cerevisiae* and software approaches that improve the build and test process. Specifically, we designed, built, and tested a synthetic bistable switch in yeast. To demonstrate the applicability of the switch as a functional module, we built a rewritable antibiotic resistance memory, which employs the switch as a component of its circuit architecture. To develop an oscillator in yeast, we designed an auxin-sensitive relaxation oscillator, performed mathematical modeling and

analysis, and proposed a high-throughput method called Time-seq to tune the oscillator. To address the challenges inherent in the build and test processes, we developed and implemented a software system called Aquarium, a smart wetlab operating system that enables human-in-the-loop automation, where researchers submit orders and technicians execute experiments following instructions from Aquarium. For the build process, we developed two core cloning process in Aquarium: plasmid construction and yeast cloning. Through Aquarium, researchers view the build process as an input-output abstraction so they can instead focus on high-level designs and leave the build details to the software and technicians. For the test process, we developed a yeast cytometry process in Aquarium, where researchers submit orders to perform time course cytometry experiments with customizable media inputs, time points, and dilution rates. Researchers directly receive the cytometry results without the struggle of having to actually perform the cytometry experiment themselves. To streamline the downstream analysis, we developed a Python package named Cowfish to automatically perform data retrieval, labeling, and pre-processing of the cytometry results from Aquarium. These build and test processes in Aquarium provide a modern way of cloning and testing with repeatable, easy-to-debug, and high-throughput software-enabled human-in-the-loop automation.

TABLE OF CONTENTS

	Page
List of Figures	iii
List of Tables	viii
Chapter 1: Introduction	1
1.1 Motivation	1
1.2 Overview	2
Chapter 2: Design, Construction, and Validation of a Synthetic Bistable Switch in Yeast	4
2.1 Circuit Design	5
2.2 Experimental Results	8
2.3 Mathematical Models	9
2.4 Methods	19
2.5 Summary	20
Chapter 3: Design, Construction, and Validation of a Rewritable Antibiotic Resistance Memory in Yeast	22
3.1 Circuit Design	22
3.2 Experimental Results	23
3.3 Mathematical Models	23
3.4 Methods	29
3.5 Summary	32
Chapter 4: Design, Analysis, and High-throughput Testing Method of an Auxin-Sensitive Relaxation Oscillator in Yeast	33
4.1 Introduction	33
4.2 ASRO design	33

4.3 Mathematical Models	34
4.4 Requirements for Sustained Oscillations	37
4.5 High-throughput Testing Method: Time-seq	44
4.6 Discussion	47
4.7 Summary	47
 Chapter 5: Build and Test the Aquarium Way	49
5.1 Aquarium	50
5.2 Build the Aquarium Way: Plasmid Construction and Yeast Cloning	52
5.3 Test the Aquarium Way: Yeast Cytometry and Cowfish	58
5.4 Summary	61
 Chapter 6: Conclusions	62
 Bibliography	64
 Appendix A: Plasmids and Yeast Strains	70

LIST OF FIGURES

Figure Number	Page
2.1 ZAVNY and ZEV chimeric protein design schematics (a) ZAVNY consists of five subunits and is a novel fluorescent, auxin degradable transcriptional activator that activates pGALZ promoter. (b) ZEV consists of three subunits and works as a β -e inducible transcriptional activator.	6
2.2 Circuit diagram and experimental data of the bistable switch. (a) Circuit diagram of the synthetic bistable switch in yeast. Both TIR1DM and ZEV are driven by constitutive yeast promoters: pACT1 and pGPD. ZAVNY is degraded in the presence of auxin by TIR1DM. (b) Circuit diagram of the control strain without positive feedback. ZAVNY is replaced with EYFP. (c) Circuit diagram of the control strain without auxin receptor. Auxin cannot degrade ZAVNY in this circuit. (d, e, f) Time-course cytometry experiment data for the bistable switch and its controls under a variety of inputs. Model fit corresponds to the model in Figure 2.4. (d) Experiment data for the bistable switch under cycled inputs 10, 00, 01, 00 to show that the switch can be switched on and off repeatedly. (e) Experiment data for the bistable switch and control without positive feedback under inputs 10, 00 to show the long-term ON state stability. (f) Experiment data for the bistable switch and control without auxin receptor under inputs 10, 00, 01, 00 to show the long-term off state stability.	7
2.3 Biochemical reaction network of the synthetic bistable switch in yeast. A is the ZAVNY, B is the ZEV, F is the TIR1DM, B^* is ZEV bound by β -e, and F^* is the TIR1DM bound by auxin. G_a is A's coding gene that not being activated. G_{aa} and G_{ab} are G_a that being bound by A and B^* , which are activated and can be transcribed and translated to A with different rates α_{aa} and α_{ab} . G_b and G_f are genes coding for B and F which are constitutively expressed. B turns into B^* with rate $\omega_b v$, where v is the concentration of β -e. F turns into F^* with rate $\omega_f u$, where u is the concentration of auxin. A_f is the protein complex formed by A and F^* , where A in the complex is subjected to protein ubiquitination. The rest of the interactions and rate parameters are self-explanatory by inspection of the graph.	10

2.4	Simplified circuit diagrams and mathematical models of three experimental yeast strains (a) bistable switch, (b) the control strain without positive feedback, and (c) the control strain without auxin receptor. In the ODEs, A is the concentration of ZAVNY, Y is the concentration of EYFP, v is the concentration of β -e and u is the concentration of auxin. Parameters in these equations are explained in Table 2.1	11
2.5	Bifurcation diagram when varying concentrations of either β -e or auxin for (a) the bistable switch, (b) the control circuit without positive feedback, and (c) the control circuit without auxin receptor.	16
2.6	Bifurcation diagrams for the bistable switch system for parameters k_0 , k_2 , k_4 , and n . The dots and circles indicate the stable and unstable equilibriums under the estimated parameter values.	18
3.1	A rewritable antibiotic resistance memory (ReARM) in yeast. (a) Circuit diagram of the ReARM in yeast. (b) Circuit diagram of the control strain without the bistable switch circuitry. (c, d, e, f) Growth rate and growth curve of ReARM and the control strain without bistable switch under series of inputs. (c) Experimental data showed the switchability of the resistance memory. Cells were grown in $400 \mu\text{g/mL}$ Zeocin media plus respective inducers determined by the inputs. Growth rate was high with input 10, kept high with input 00, changed to low with input 01, kept low with input 00, and changed to back to high with input 10. (d) Experimental data showed ON state stability of the resistance memory. Growth rate kept high after input 10 with at least four steps of 00. (e) Experimental data demonstrating the OFF state stability of the resistance memory, noting that the strains were induced with $20 \mu\text{M}$ auxin to switch to OFF state before 0 h. (f) Experimental data showed that control strain without bistable switch did hold ON state. The growth rate dropped from high to low after input 10 was changed to input 00 at 20 h. . .	24
3.2	Simplified circuit diagram and mathematical models of two experimental yeast strains (a) ReARM, and (b) the control strain without the bistable switch.	25
3.3	Biochemical reaction network of the ReARM. A is ZAVNY, B is ZEV, F is TIR1DM, E is BleoMX, B^* is ZEV bound by β -estradiol, and F^* is the TIR1DM bound by auxin. Additional to what described in Figure 2.3, G_e is E's coding gene that not being activated. G_{ea} and G_{eb} are G_e that being bound by A and B^* , which are activated and can be transcribed and translated to A with different rates α_{ea} and α_{eb} . The rest of the interactions and rate parameters are self-explanatory by inspection of the graph.	27

3.4 Model prediction and growth curve fitting for the time course plate reader assay. Red line in each figure shows the model fit with parameters estimations shown in Table 3.1. Model predicted ZAVNY and BloeMX concentration dynamics are shown in the upper portion of each subfigure.	30
4.1 The ASRO design (a) Circuit diagram of the auxin-sensitive relaxation oscillator (ASRO), where ASTA is an auxin-sensitive transcription activator and FBox is an F-Box protein. ASTA activates the synthesis of both ASTA and FBox, while FBox degrades ASTA in the presence of the plant hormone auxin. (b) ASTA schematic design consists of four protein domains and a fused fluorescence protein. Domain I, II, IV together realize the transcriptional activating function of the chimeric protein. Domain II is an auxin degron, which makes the protein subject to auxin induced degradation by FBox.	34
4.2 Biochemical reaction network of the ASRO. A is short for ASTA and F is short for FBox for simple illustrations. G_A and G_F are genes coding for A and F that are not activated by A, while G_A^* and G_F^* are genes that are activated by A. M_A and M_F are mRNAs that code for A and F. C is the protein complex formed by A and F through protein interactions induced by auxin. A is targeted by ubiquitin for protein degradation in the complex C hence $C \xrightarrow{\delta_C} F$. Rate parameters in this biochemical reaction network are self-explanatory by inspection of the graph. We assume that the transcription rates caused by activator A is greater than the leaky expression, thus having $\alpha_A > \alpha_A^*$ and $\alpha_F > \alpha_F^*$. Also noting that rate γ_C is dependent on auxin concentration.	35
4.3 Sustained oscillations requirements analysis. (a) A simple phase plane graph on the Poincaré-Bendixson boundaries to explain that the system is confined in a bounded region. (b) Graphical illustration shows that the system has a single equilibrium when Hill coefficient $n = 1$. (c) Numerical simulations show that the system is non-oscillatory when $n = 1$. (d) Numerical simulations produce sustained oscillations when Hill coefficient $n = 2$. The other parameters used in the two simulations are $\lambda_A = 0.08, \pi_A = 1.9, \rho_A = 0.01, \lambda_F = 0.002, \pi_F = 0.058, \rho_F = 0.01, \gamma_C = 0.025$, and $\delta_A = \delta_F = 0.0045$. These parameters are randomly chosen within a sensible biophysical range.	41

4.4	Changing the DNA binding affinity tunes the dynamical behavior of system S . a-d all assume that $\rho_A = \rho_F = \rho$. Numerical simulations show the dynamical behavior of system S when changing ρ from 0 to 0.05 while other parameters are held to their nominal values of $\lambda_A = 0.08, \pi_A = 1.9, \lambda_F = 0.002, \pi_F = 0.058, \gamma_C = 0.025$, and $\delta_A = \delta_F = 0.0045$. From simulation results we can see that $\rho = 0.01$ gives sustained oscillations but other parameter choices give either steady states ($\rho = 0$ or 0.05) or damped oscillations ($\rho = 0.002$). We obtained similar simulation results by changing parameter γ_C .	42
4.5	Root locus analysis of system S with respect to parameters $\rho_A = \rho_F = \rho$ and γ_C . (a) Numerical simulations show how the eigenvalues of system S change when changing parameter ρ from 0 to 0.5 with a step size of 0.0001. We marked out corresponding eigenvalues of system S when $\rho = 0, 0.002, 0.01$, and 0.05. We see that the real parts of the eigenvalues when $\rho = 0.01$ are all positive, which satisfy conditions (i) and (ii), thus giving rise to sustained oscillations, while real parts of eigenvalues of $\rho = 0, 0.002, 0.05$ are all negative, thus generating stable solutions. These results can be cross-checked by numerical simulations in Figure 4.4. (b) Numerical simulations show how eigenvalues of system S change when changing parameter γ_C from 0 to 1 with a step size of 0.0001. We see that there is a range of γ_C where the real parts of eigenvalues are positive, which leads the system to display sustained oscillations. These two simulations inform us that tuning the DNA binding affinity and the auxin degradation strength in the ASRO could push the system into a sustained oscillatory regime.	43
4.6	Overview of the Time-seq method workflow	46
5.1	Aquarium overview: researchers design and technicians build	50
5.2	Aquarium inventory scheme. (a) The inventory scheme overview. (b) An <i>Item</i> with <i>Container Type</i> of <i>Plasmid Stock</i> and <i>Sample</i> of <i>Plasmid pGALZ4-BleoMX</i> . (c) An <i>Item</i> with <i>Container Type</i> of <i>Glycerol Stock</i> and <i>Sample</i> of <i>Plasmid pGALZ4-BleoMX</i> . (d) An <i>Item</i> with <i>Container Type</i> of <i>Glycerol Stock</i> and <i>Sample</i> of <i>Yeast Strain pGALZ4-BleoMX</i> in W303a. (e) An <i>Item</i> with <i>Container Type</i> of <i>Stripwell</i> and has a 1x8 <i>Sample</i> array. (f) An <i>Item</i> with <i>Container Type</i> of <i>96-Well Plate</i> and has an 8x12 <i>Sample</i> array.	53
5.3	Aquarium Krill Protocol Examples. (a) Text instructions shown to the technician on a webpage. (b) Box layout illustration to guide technician to retrieve an inventory item from a 9x9 freezer box.	54
5.4	Overview of plasmid construction process in Aquarium	56
5.5	Overview of yeast cloning process in Aquarium	58

5.6 Yeast cytometry process in Aquarium (a) Flow chart overview of the yeast cytometry process (b) Example of a possible dilution read schedule.	59
5.7 Cowfish Dataframe Example. The dataframe is indexed by the absolute time that sample was passed through the cytometer. <i>conc</i> stands for the concentration of the processed yeast sample, <i>events</i> stands for number of events detected, <i>FL1A_mean</i> is the mean of the fluorescence data reported by the cytometer, <i>FL1A_sd</i> is the standard deviation, <i>vol</i> is the volume of the samples passed in the cytometer, <i>sample_name</i> and <i>inducer_condition</i> are information retrieved from the Aquarium job log and automatically aligned with the cytometry data.	60

LIST OF TABLES

Table Number	Page
2.1 Description, estimation, and unit of parameters shown in the mathematical models. The estimation values of the parameters are from the model fit of experimental data shown in Figure 2.2d,e,f	17
3.1 Description, estimation, and unit of parameters shown in the mathematical models. The estimation values of the parameters are from the model fit of experimental data shown in Figure 3.4	31
A.1 Plasmids with descriptions and publicly accessible Benchling links. The specific Zinc finger binding domain used in the bistable switch, ReARM and related circuits is coded as Z4 (short as Z in main text). The pGALZ4 and Z4AVNY refer to pGALZ and ZAVNY in the main text respectively.	70
A.2 Yeast strains with descriptions along with the plasmids integrated into their genome.	71

ACKNOWLEDGMENTS

I would like to start my acknowledgments with deep appreciation and thanks to my advisor Prof. Eric Klavins. I began my adventure in synthetic biology when I took Eric's Introduction to synthetic biology class in Fall 2011, where I was introduced to cutting edge synthetic biology research through Eric's charming lectures with personal hand written and drawn lecture notes. Eric advised me that my background in electrical engineering could make an unique impact in synthetic biology. He then granted me the opportunity to work on a project to characterize a synthetic circuit in yeast using fluorescence microscopy to create a frequency Bode plot, and I have been working in the Klavins Lab since then. Throughout my PhD years, Eric provided me with invaluable guidance and support. I am most grateful for Eric's encouragement and confidence in my ability to propose and execute a project as an independent researcher and engineer. I am very thankful for Eric's enthusiasm in joining his lab at the beginning of my PhD journey, and for being a thoughtful, supportive, and brilliant advisor ever since.

I thank my committee members, Prof. Jennifer Nemhauser, Prof. Georg Seelig, and Prof. James Carothers, for their invaluable advice and the time and energy they invested into the success of my graduate career and beyond. In particular, I would like to thank Jennifer, who has advised me since the beginning of my PhD research when I became involved in the Auxin project. Her advice is always insightful and right to the point, and I also appreciate her guidance in my career development before I began my job search.

I thank the members of Klavins lab who welcomed me with their whole hearts when I first joined the lab and advised and supported me since: Josh Bishop, Fayette Shaw, Rob Egbert, Kevin Oishi, Chris Takahashi, and Shelly Jang. These colleagues set the example that I

strived to follow throughout my graduate studies, and guided me through steps towards my future career. I also thank Kyle Havens, who was a postdoc when I joined the lab, and who guided me through my introduction to biology by teaching me the best practices for wetlab experiments. I thank my fellow PhD students, Nick Bolten, David Younger, Miles Gander, Tileli Amimeur, Leandra Brettner, Arjun Khakhar, and Justin Vrana, all of whom I was very lucky to work alongside with in tackling the challenges of synthetic biology. I also thank postdocs Alberto Carignano, Orlando de Lange, and Laura Adam, who shared with me their expertise and enthusiasm, and helped me succeed in my PhD career.

Special thanks Michelle Parks, the lab manager of Klavins Lab and the UW BIOFAB, who I was so fortunate to work with closely in building the Aquarium cloning workflows. Her enthusiasm, dedication, and professionalism made the successful implementation of the semi-automated Aquarium cloning workflows which benefited tens of researchers. The UW BIOFAB could not have been built without her.

I would like to particularly thank Alberto Carignano, Miles Gander, Michelle Parks, and David Younger for their diligent review and edits on this thesis. They spent so many hours helping me rewriting sentences and paragraphs to conform to the highest standards.

I thank my dear friends Xiaofeng, Sa, Jingren, Junlin, and Xudong, who I spent many evenings with during my second and third years cooking and enjoying dinner together. I will forever cherish those nights and the friendship we carried beyond.

I would like to thank my parents, who raised me with their hard work and sacrifices, who love and support me no matter where I am or what I do. I would like to thank my older brother, who set an excellent example for me as a surgeon. I probably would not have come to the United States to pursue a PhD without his encouragement and support. Lastly, I would like to thank my wife, for her unwavering love and faith and me, who I was so lucky to marry. She gives me happiness everyday, and I am blessed to start a family with her. Thank you and I love you!

DEDICATION

To my parents for their love and sacrifice.

To my wife Dian.

You are my everything.

Chapter 1

INTRODUCTION

1.1 Motivation

Cells are dynamical systems governed by underlying genetic programs and interactions with the surrounding environment. In synthetic biology, researchers design, build, and test synthetic gene circuits with the aim to gain a deeper understanding of the fundamental mechanisms underlying biological systems, and improve our ability to engineer biological systems for useful purposes [46]. Many of these synthetic gene circuits are engineered dynamical systems that exhibit designed properties. For example, of the two gene circuits that marked the beginning of synthetic biology, one is a bistable switch in *E.coli* and the other is an oscillator in *E.coli*, both are dynamic circuits resulted from designed genetic programs. Since the foundation of synthetic biology, researchers have built various dynamic gene circuits *in vivo*, including bistable switches [36], oscillators [7, 19, 53, 55], synchronized oscillators [13], timers [15], counters [18], and logic gates [41, 58].

However, most of the dynamic gene circuits were realized in *E.coli*. Yeast, a model eukaryote and widely used by humans for millennia, is of great interest to synthetic biology, both as a platform for understanding eukaryote and also engineering for industrial use [10]. Synthetic biologists have been building circuits and engineering metabolic pathways in yeast for decades [6, 8, 49]. However, it remains challenging to design, build, and test dynamic gene circuits in yeast. For example, there has not been a published report of a switchable bistable switch or an oscillator in yeast, while the bistable switch and oscillator were built in *E.coli* over a decade ago. The eukaryotic nature of yeast means that its gene regulation is not as predictable as in *E.coli*. Limited number of standardized and orthogonal parts makes

engineering gene circuits in yeast harder than in *E.coli* [10].

Challenges also lie in the build and test process of engineering dynamic gene circuits. Most academic lab practices heavily rely on expert knowledge, are error-prone, low throughput, and difficult to debug. The build process is largely composed of molecular cloning, which most researchers carry out individually. This cloning process is often labor intensive, prone to error, and low throughput. The test process also requires expert knowledge for scientific instruments and experimental protocols. Many experimental processes in the build and test components are not well documented as they are carried out, which results in reproducibility issues. [9]. There have been several industrial efforts to solve these problems using specialized robotics and software [11]. However, it remains challenging in academic settings, where specialized robotics are too expensive.

1.2 Overview

In this thesis, we present the design, analysis, results, and novel methods for engineering dynamic gene circuits in yeast, and software approaches to improve the build and test processes. In Chapter 2, we present the design, construction, and validation of developing a bistable switch as a major milestone in building dynamic gene circuits in yeast. We present experimental results that demonstrate the bistability and switchability of the switch, and develop mathematical models that fit the experimental data and explain the stability of the switch. In Chapter 3, we present works on a rewritable antibiotic resistance memory (ReARM) built upon the bistable switch as an application of the switch. We show growth data from time course plate reader assays with a series of inputs to demonstrate the functionality of ReARM and develop mathematical models as an extension to the bistable switch model to fit the growth data. In Chapter 4, we present the design and analysis of an auxin-sensitive relaxation oscillator (ASRO) in yeast. We also propose a high-throughput testing method called Time-seq, which can be used to tune the ASRO to oscillate. In Chapter 5, we present “Build and Test the Aquarium Way”, and show how we improved the build and test processes with a software-enabled human-in-the-loop automation platform that makes

engineering dynamic gene circuits in yeast easier. Chapter 7 concludes the thesis with the summary of each chapter and suggestions on future directions.

Chapter 2

DESIGN, CONSTRUCTION, AND VALIDATION OF A SYNTHETIC BISTABLE SWITCH IN YEAST

Genetic bistable switches are one fundamental type of dynamic gene circuits. In biological systems, bistable switches play a key role in the cellular differentiation in multicellular organism [25, 59, 60], cell signaling in stem cells [35], cell cycle regulation [37, 52], phenotypic variation in bacteria [51], and more. In traditional engineering disciplines, the ability to build bistable switches has been fundamental for the engineering of complex electronic and mechanical systems [12, 28]. With the development of synthetic biology, constructing bistable switches is among the first steps towards engineering complex biological systems [32, 47]. Synthetic bistable switches have been realized in *E. coli* [20] and mammalian cells [34, 36].

Yeast, a model eukaryote and widely used by humans for several millennia, is of great interest to synthetic biology both as understanding eukaryotic system and engineering for industrial use [10]. Synthetic biologists have been building circuits and engineering metabolic pathways in yeast for decades [6, 8, 49]. However, it remains challenging to construct a functional bistable switch in yeast. The eukaryotic nature of yeast means that its gene regulation is not as simple as in *E. coli*. Less standardized, orthogonal parts make engineering synthetic circuits much harder in yeast [10]. Here, we built the first synthetic bistable switch in the yeast *S. cerevisiae*. In this chapter, we describe the design of the switch, which is based on a positive feedback loop using a novel transcriptional activator and two components for manually switching the loop on and off with two chemical inducers: β -estradiol (β -e) and auxin. We built this bistable switch and experimentally showed that the switch could be switched repeatedly on with the addition of β -e and off with auxin, and maintained either state when no inducer was present. We also built a mathematical model to fit the

experimental data and studied the stability of the system.

2.1 Circuit Design

The core of the synthetic bistable switch in yeast is a positive feedback loop using a novel transcriptional activator (Figure 2.2.a). The transcriptional activator, ZAVNY, is a chimeric protein we designed that works as a fluorescent transcriptional activator and is degradable by auxin, a plant hormone. ZAVNY consists of five domains: Zinc finger DNA binding domain (ZDBD), Auxin degron, VP16 activation domain, Nuclear Localization Signal (NLS), and Enhanced Yellow Fluorescent Protein (EYFP) (Figure 2.1). The ZDBD guides the binding to pGALZ promoter, a variant of the native yeast promoter pGAL1 with binding sites replaced with zinc finger recognition site to reduce interference with the native yeast system [39, 40]. VP16 acts as an activator. The NLS (2x SV40) enables access to the nucleus, which is critical to perform transcriptional regulatory activities in eukaryotic cells like yeast. The auxin degron, a protein subdomain from the IAA family of *Arabidopsis thaliana*, makes ZAVNY degradable by an auxin receptor protein (TIR1 or AFB2, both in FBox family) from *Arabidopsis thaliana* in the presence of the plant hormone auxin [26]. EYFP is also included to make the protein fluorescent. As a result, ZAVNY works as a fluorescent, auxin degradable transcriptional activator targeting the pGALZ promoter. A positive feedback loop on the activator introduces bistability based on previous theoretical studies [29, 30]. Theoretically, turning on the feedback loop would produce an 'on' stable state and turning off the feedback loop would produce an 'off' stable state under certain parameter constraints. However, how to externally turn on or off the positive feedback loop to switch the 'on' or 'off' states remains challenging when developing such circuits in synthetic biology [6]. The versatile functionality of ZAVNY as both an activator and auxin degradable protein provides a solution.

We designed the switch to use two chemical inducers β -estradiol (β -e) and auxin to turn the positive feedback loop on and off. In the bistable switch circuit, we introduced two components ZEV and TIR1DM, to control the positive feedback loop (Figure 2.2.a). ZEV is

a widely used β -e inducible transcriptional activator [40]. β -e induces ZEV to activate the pGALZ promoter, thus turning the positive feedback loop on. TIR1DM is a mutant variant of the auxin receptor TIR1 with a faster degradation rate [61]. Auxin induces TIR1DM to degrade ZAVNY, thus turning the positive feedback loop off. Both ZEV and TIR1DM are driven by constitutive yeast promoters, and thus are constantly expressed. Inducing the circuit with β -e or auxin should directly control the on/off of the positive feedback loop. Time course cytometry experiments shown in the results section demonstrate that the circuit works as expected.

In order to develop a bistable switch that can be used for a variety of applications, the switch must be modular and easily tunable. The switch described here achieves modularity by regulating a promoter, pGALZ, which can be used to drive the expression of any gene of interest. Tunability is achieved by swappable domains. The Z4 DNA binding domain is interchangeable with other zinc finger binding domains or other functional DNA binding domains, as long as a compatible promoter is used instead of pGALZ. The auxin degron domain of ZAVNY can be swapped with a library of auxin degrons or full length IAAAs from *Arabidopsis thaliana* [26, 31]. Other FBoxes with different dynamics can be used instead of TIR1DM [26, 31].

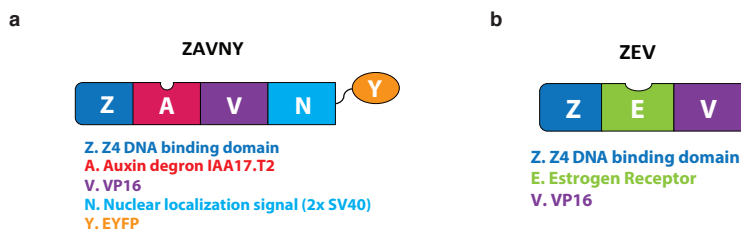


Figure 2.1: ZAVNY and ZEV chimeric protein design schematics (a) ZAVNY consists of five subunits and is a novel fluorescent, auxin degradable transcriptional activator that activates pGALZ promoter. (b) ZEV consists of three subunits and works as a β -e inducible transcriptional activator.

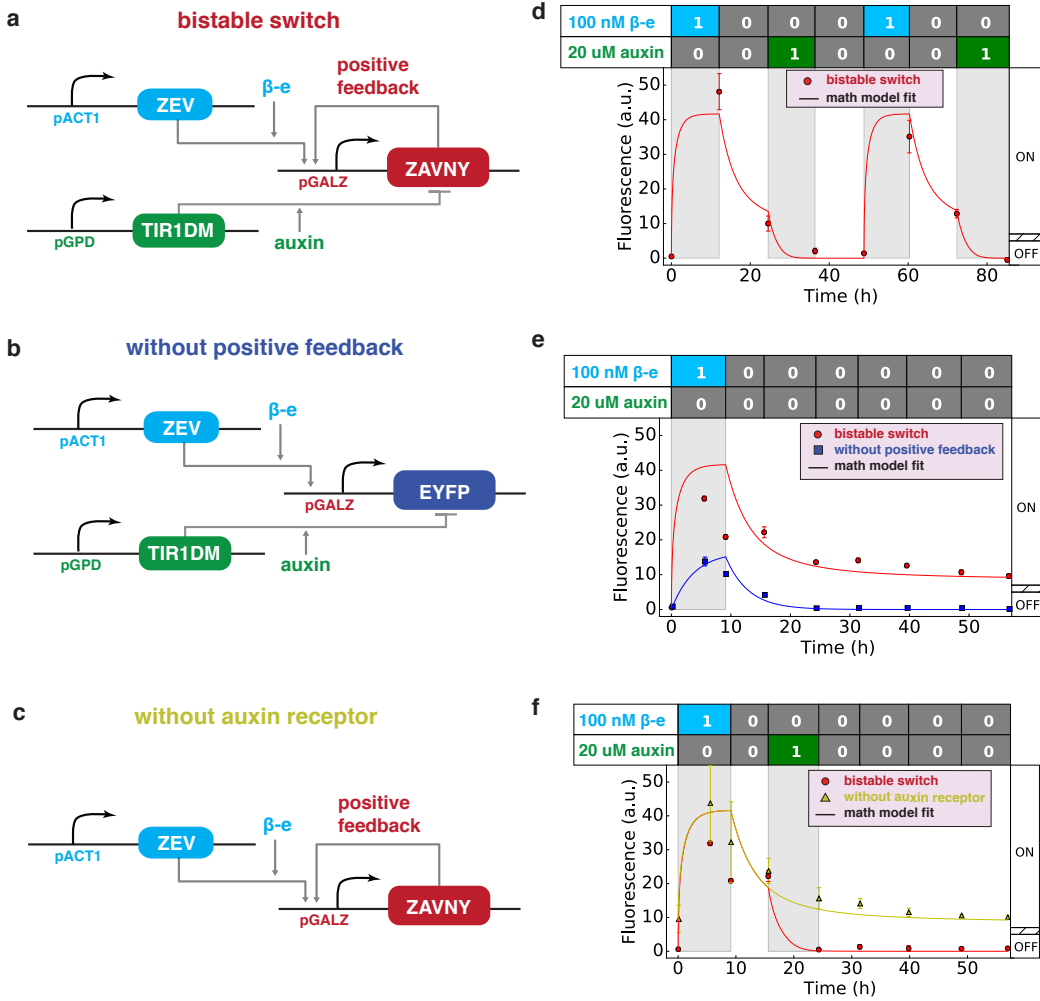


Figure 2.2: Circuit diagram and experimental data of the bistable switch. (a) Circuit diagram of the synthetic bistable switch in yeast. Both TIR1DM and ZEV are driven by constitutive yeast promoters: pACT1 and pGPD. ZAVNY is degraded in the presence of auxin by TIR1DM. (b) Circuit diagram of the control strain without positive feedback. ZAVNY is replaced with EYFP. (c) Circuit diagram of the control strain without auxin receptor. Auxin cannot degrade ZAVNY in this circuit. (d, e, f) Time-course cytometry experiment data for the bistable switch and its controls under a variety of inputs. Model fit corresponds to the model in Figure 2.4. (d) Experiment data for the bistable switch under cycled inputs 10, 00, 01, 00 to show that the switch can be switched on and off repeatedly. (e) Experiment data for the bistable switch and control without positive feedback under inputs 10, 00 to show the long-term ON state stability. (f) Experiment data for the bistable switch and control without auxin receptor under inputs 10, 00, 01, 00 to show the long-term off state stability.

2.2 Experimental Results

To test the switch, we developed an assay in which yeast were grown in one of each of three types of media representing the possible inputs to the switch. The input 00 was implemented with plain synthetic complete (SC) media, the input 10 was implemented with SC media containing 100 nM β -e, and the input 01 was implemented with SC media containing 20 μ M auxin. To apply a particular input, cells were diluted to 1 event/ μ L. Short applications of an input (10-12 hours) show simple growth, whereas in longer applications, cells were periodically diluted with the same media to keep them growing around log phase.

Starting in the OFF state, the switch (Figure 2.2a) was switched into the ON state, indicated by high fluorescence (Figure 2.2e), via 11 hours of growth with input 10. Upon application of input 00, the switch remained in the ON state for at least 47 hours (Figure 2.2e), whereas the no-positive-feedback control (Figure 2.2b) returned to basal levels of fluorescence within ten hours under the same conditions. Steady state fluorescence levels were observed to be higher in β -e media than after dilution with plain media, likely due to extra activation of ZAVNY by ZEV, which is consistent with our model (described below).

Starting in the ON state and growing in input 00, the switch was switched into the OFF state, indicated by low fluorescence (Figure 2.2f), via application of input 01. The switch returned to basal level within six hours. Upon application of input 00 after 12 hours, the switch cells remained OFF for at least 32 hours (Figure 2.2f). In contrast, a control strain without the auxin receptor TIR1DM (Figure 2.2c), could not be turned off (Figure 2.2f) via the application of input 01.

The switch was cycled between the ON and OFF states twice, in an 85 hour experiment, by alternating between the inputs 10, 00, 01, and 00 twice. We observed essentially the same behavior in each cycle (Figure 2.2d), with the switch on for the first half of each cycle, and off for the second half of each cycle.

2.3 Mathematical Models

In order to describe the behavior of the bistable switch and its controls, we developed simple mathematical models, performed bistability analysis, and model prediction for the switch (Figure 2.4a), the control circuit without positive feedback (Figure 2.4b), and the control circuit without the auxin receptor (Figure 2.4c). First, we show the derivation of the model from a full mechanistic model of the reactions involved to a one-dimensional model using mass conservation and quasi steady state assumptions (Figure 2.3). For the model prediction, parameters were first estimated using the data shown in Figure 2.2b,e,f, and are listed in Table 2.1. Based on the estimated parameters, we performed bifurcation analysis by studying how varying β -e and auxin inputs changed the stability profile and how it matched with the experimental results. Lastly, we explored how varying certain parameters in the model could change the stability profile of the switch and discussed possible strategies for tuning the switch.

2.3.1 Model Derivation

Bistable Switch Circuit

The bistable switch circuit can be modeled through the biochemical reaction network shown in Fig. 2.3, where we drew a schematic network of how genes and proteins interact in the circuit and gave their corresponding chemical equations. We did not specifically model the mRNA in this network. The parameters $\alpha_{aa}, \alpha_{ab}, \alpha_b, \alpha_f$ are lumped parameters that describe the net effect of transcription and translation. All rate parameters are positive real numbers. Assuming mass action kinetics, the temporal dynamics of this system are given by

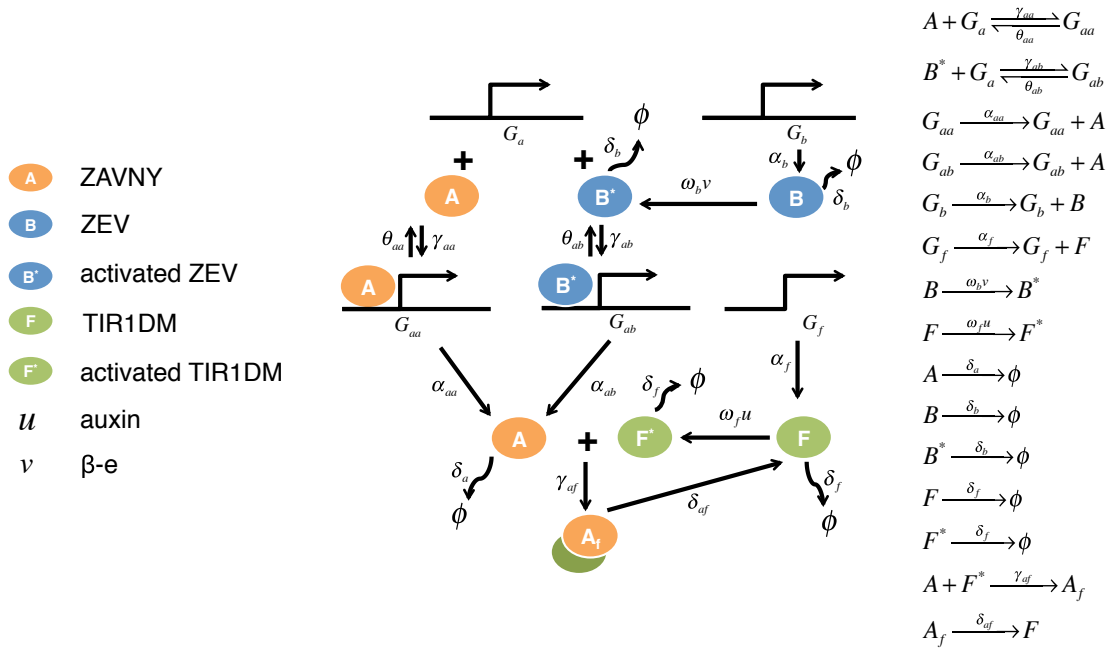


Figure 2.3: Biochemical reaction network of the synthetic bistable switch in yeast. A is the ZAVNY, B is the ZEV, F is the TIR1DM, B^* is ZEV bound by $\beta\text{-e}$, and F^* is the TIR1DM bound by auxin. G_a is A's coding gene that not being activated. G_{aa} and G_{ab} are G_a that being bound by A and B^* , which are activated and can be transcribed and translated to A with different rates α_{aa} and α_{ab} . G_b and G_f are genes coding for B and F which are constitutively expressed. B turns into B^* with rate $\omega_b v$, where v is the concentration of $\beta\text{-e}$. F turns into F^* with rate $\omega_f u$, where u is the concentration of auxin. A_f is the protein complex formed by A and F^* , where A in the complex is subjected to protein ubiquitination. The rest of the interactions and rate parameters are self-explanatory by inspection of the graph.

a bistable switch

$$\frac{dA}{dt} = \frac{k_0 A^n + k_1 v}{1 + k_2 A^n + k_3 v} - k_4 A - \frac{k_5 u A}{1 + k_6 A + k_7 u}$$

b without positive feedback

$$\frac{dY}{dt} = k_8 \frac{k_1 v}{1 + k_3 v} - k_4 Y$$

c without auxin receptor

$$\frac{dA}{dt} = \frac{k_0 A^n + k_1 v}{1 + k_2 A^n + k_3 v} - k_4 A$$

Figure 2.4: Simplified circuit diagrams and mathematical models of three experimental yeast strains (a) bistable switch, (b) the control strain without positive feedback, and (c) the control strain without auxin receptor. In the ODEs, A is the concentration of ZAVNY, Y is the concentration of EYFP, v is the concentration of β -e and u is the concentration of auxin. Parameters in these equations are explained in Table 2.1

the reaction rate equations as follows

$$\begin{aligned}
\frac{dG_a}{dt} &= \theta_{aa}G_{aa} + \theta_{ab}G_{ab} - \gamma_{aa}G_aA - \gamma_{ab}G_aB^* \\
\frac{dG_{aa}}{dt} &= \gamma_{aa}G_aA - \theta_{aa}G_{aa} \\
\frac{dG_{ab}}{dt} &= \gamma_{ab}G_aB^* - \theta_{ab}G_{ab} \\
\frac{dA}{dt} &= -\gamma_{aa}G_aA + \theta_{aa}G_{aa} + \alpha_{aa}G_{aa} + \alpha_{ab}G_{ab} - \gamma_{af}AF^* - \delta_aA \\
\frac{dB}{dt} &= \alpha_bG_b - \delta_bB \\
\frac{dB^*}{dt} &= -\gamma_{ab}G_aB^* + \theta_{ab}G_{ab} + \omega_bvB - \delta_bB^* \\
\frac{dF}{dt} &= \alpha_fG_f + \delta_{af}A_f - \omega_fuF - \delta_fF \\
\frac{dF^*}{dt} &= \omega_fuF - \gamma_{af}AF^* - \delta_fF^* \\
\frac{dA_f}{dt} &= \gamma_{af}AF^* - \delta_{af}A_f,
\end{aligned} \tag{2.1}$$

where $G_a, G_{aa}, G_{ab}, A, B, F, B^*, F^*, A_f$ represent the concentrations of these species shown in Figure 2.3. Assuming quasi-steady-state for $G_a, G_{aa}, G_{ab}, B, B^*, F, F^*, A_f$, we set all corresponding rate equations to be zero. Assuming that the gene copy number for A, B and F are 1 for the simplicity of the model without losing generality, we get $G_a + G_{aa} + G_{ab} = 1$, $G_b = 1$ and $G_f = 1$.

The following equations hold based on the assumptions:

$$\begin{aligned}
& \theta_{aa}G_{aa} + \theta_{ab}G_{ab} - \gamma_{aa}G_aA - \gamma_{ab}G_aB^* = 0 \\
& \gamma_{aa}G_aA - \theta_{aa}G_{aa} = 0 \\
& \gamma_{ab}G_aB^* - \theta_{ab}G_{ab} = 0 \\
& \alpha_b - \delta_bB = 0 \\
& -\gamma_{ab}G_aB^* + \theta_{ab}G_{ab} + \omega_bvB - \delta_bB^* = 0 \\
& \alpha_f + \delta_{af}A_f - \omega_fuF - \delta_fF = 0 \\
& \omega_fuF - \gamma_{af}AF^* - \delta_fF^* = 0 \\
& \gamma_{af}AF^* - \delta_{af}A_f = 0 \\
& \frac{dA}{dt} = -\gamma_{aa}G_aA + \theta_{aa}G_{aa} + \alpha_{aa}G_{aa} + \alpha_{ab}G_{ab} - \gamma_{af}AF^* - \delta_aA \\
& G_a + G_{aa} + G_{ab} = 1 \\
& G_b = 1 \\
& G_f = 1.
\end{aligned} \tag{2.2}$$

After mathematical derivations, we get the dynamics for A as

$$\frac{dA}{dt} = \frac{\lambda_aA + \lambda_b\pi_bv}{1 + \rho_aA + \rho_b\pi_bv} - \delta_aA - \frac{\lambda_f\gamma_{af}Au}{\delta_f + \gamma_{af}A + \omega_fu}, \tag{2.3}$$

where $\lambda_a = \frac{\gamma_{aa}}{\theta_{aa}}\alpha_{aa}$, $\lambda_b = \frac{\gamma_{ab}}{\theta_{ab}}\alpha_{ab}$, $\rho_a = \frac{\gamma_{aa}}{\theta_{aa}}$, $\rho_b = \frac{\gamma_{ab}}{\theta_{ab}}$, $\pi_b = \frac{\omega_b}{\delta_b^2}\alpha_b$, and $\lambda_f = \frac{\omega_f\alpha_f}{\delta_f}$.

To model the cooperativity of ZAVNY in gene activation, we generalize Equation 2.3 as follows,

$$\frac{dA}{dt} = \frac{\lambda_aA^n + \lambda_b\pi_bv}{1 + \rho_aA^n + \rho_b\pi_bv} - \frac{\lambda_f\gamma_{af}Au}{\delta_f + \gamma_{af}A + \omega_fu} - \delta_aA \tag{2.4}$$

where n is the Hill coefficient and $n > 0$.

By renaming parameters as k_0 to k_n for easier communication, we have the following:

$$\frac{dA}{dt} = \frac{k_0 A^n + k_1 v}{1 + k_2 A^n + k_3 v} - k_4 A - \frac{k_5 u A}{1 + k_6 A + k_7 u}. \quad (2.5)$$

Inspecting the right-hand side of Equation 2.4, there are three terms; we can see that the first term models the activation of A by auto-induction and β -e induction. The second term models the basal degradation and dilution of A. The third term models auxin induced degradation of A.

The Control Circuit without Positive Feedback

The control circuit without positive feedback is shown in Figure 2.2b and Figure 2.4b. We assume that the degradation and dilution rate for EYFP are similar to those of ZAVNY. Following similar mathematical derivations, we have the 1D ODE model for the without positive feedback strain:

$$\frac{dY}{dt} = k_8 \frac{k_1 v}{1 + k_3 v} - k_4 Y, \quad (2.6)$$

where Y stands for the concentration of EYFP as in the control circuit. The parameter k_8 models the differences in synthesis rate between ZAVNY and EYFP. The first term modes the activation of Y by β -e induction. The second term models the basal degradation and dilution of Y.

The Control Circuit without Auxin Receptor

The control circuit without an auxin receptor is shown in Figure 2.2c and Figure 2.4c. Following similar mathematical derivations, we have the 1D ODE model for the without auxin receptor strain:

$$\frac{dY}{dt} = \frac{k_0 A^n + k_1 v}{1 + k_2 A^n + k_3 v} - k_4 A, \quad (2.7)$$

where the only difference compared to Equation 2.5 is that the third term that models the degradation of A in the presence of auxin is gone.

2.3.2 Model Fit and Predication

We estimate the parameters in the bistable switch model with data shown in Figure 2.2b,e,f, where the model fit was plotted with solid lines. The parameters were estimated by fitting the data to the 1D ODE model in Equation 2.5 using the downhill simplex algorithm with customized Python code. The estimated parameter values and descriptions are listed in Table 2.1.

The switch model predicts two stable equilibria for the concentration of ZAVNY, separated by an unstable equilibrium (Figure 2.5a). When the concentration of β -e is increased, the low stable equilibrium and unstable equilibrium annihilate and the high stable equilibrium increases, which results in a single, stable, and non-zero equilibrium that is higher than the high state without the β -e. When the concentration of auxin is increased, the high stable equilibrium and unstable equilibrium annihilate to produce a single stable equilibrium at zero. Thus, as shown experimentally, the model predicts that pulsing the system with β -e or auxin can push the concentration of ZAVNY from the low state to the high state, because those signals temporarily remove the unstable equilibrium between the two states that serves as a threshold. In contrast, the control circuit without positive feedback only has a single stable equilibrium that monotonically increases with the concentration of β -e (Figure 2.5b). In addition, the control without the auxin receptor cannot be switched off by auxin once turned on because the addition of auxin has no effect on the equilibrium structure (Figure 2.5c).

The model predicts that the bistable switch system will go through a saddle-node bifurcation under the following circumstances: 1) positive feedback synthesis rate parameter k_0 decreases; 2) positive feedback synthesis rate parameter k_2 increases; 3) dilution and degradation rate k_4 increases; 4) Hill coefficient n decreases. We made bifurcation diagrams (Figure 2.6.d) to study how the bistable switch stability profiles change if parameters k_0 , k_2 , k_4 , or n change. The system always has a zero stable equilibrium during the studied parameter ranges for any k_0 , k_2 , k_4 , or n . However, the appearance and the value of the stable

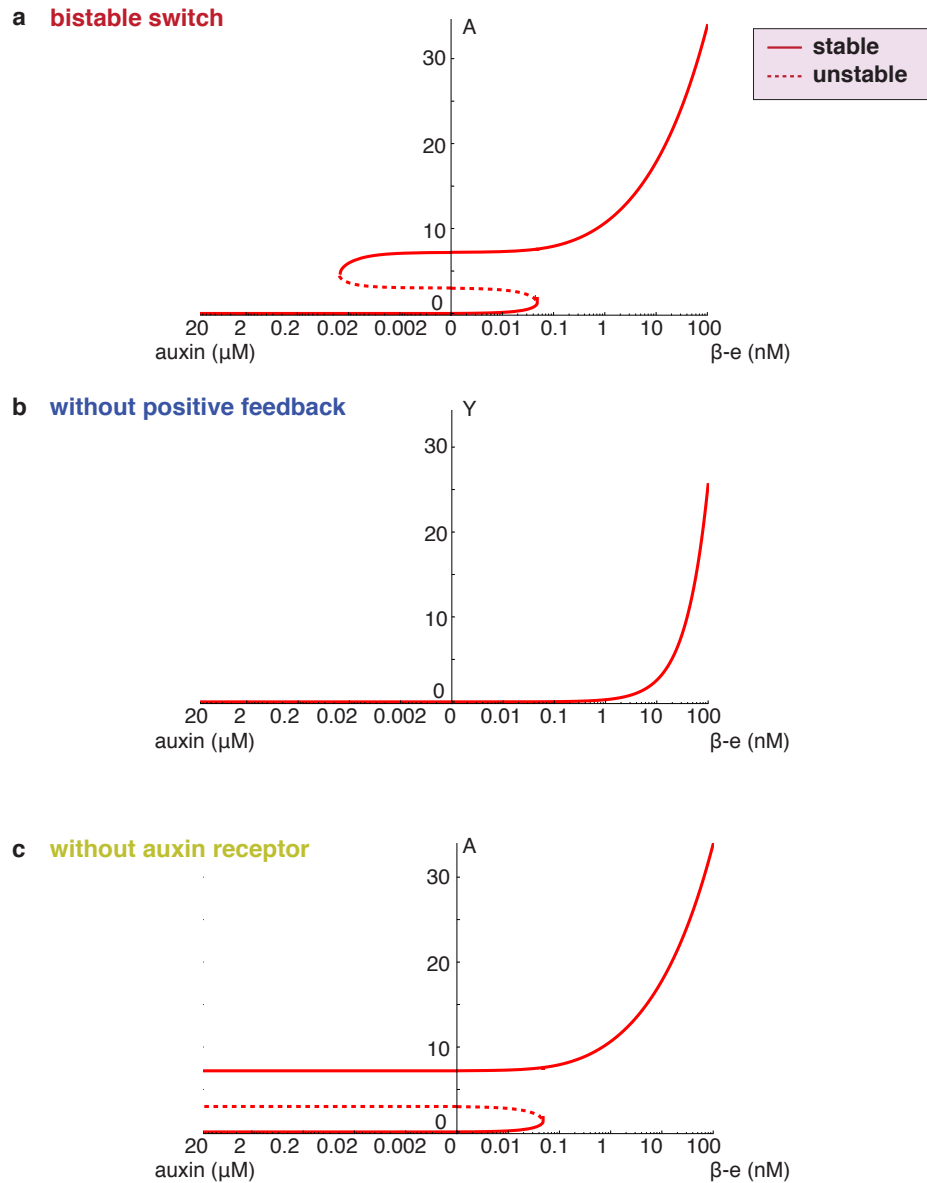


Figure 2.5: Bifurcation diagram when varying concentrations of either β -e or auxin for (a) the bistable switch, (b) the control circuit without positive feedback, and (c) the control circuit without auxin receptor.

Parameter	Description	Estimation	Units
k_0	lumped parameter related to the positive feedback activation and the synthesis rate of ZAVNY of A	0.071	$(\mu M)^{-n+1} h^{-1}$
k_1	lumped parameter related to the activation and synthesis rate of ZAVNY induced by β -e	221.852	h^{-1}
k_2	lumped parameter related to the positive feedback activation and synthesis rate of ZAVNY	0.017	$(\mu M)^{-n}$
k_3	lumped parameter related to the activation and synthesis rate of ZAVNY induced by β -e	0.002	$(\mu M)^{-1}$
k_4	dilution and degradation rate for ZAVNY	0.267	h^{-1}
k_5	lumped parameter related to the degradation rate of ZAVNY induced by auxin	5.322	$(\mu M)^{-1} h^{-1}$
k_6	lumped parameter related to the degradation rate of ZAVNY induced by auxin	0.007	$(\mu M)^{-1}$
k_7	lumped parameter related to degradation rate of ZAVNY induced by auxin	10.396	$(\mu M)^{-1}$
k_8	Difference in synthesis rate between ZAVNY and EYFP	0.02	Unitless
n	Hill coefficient for A	2	Unitless

Table 2.1: Description, estimation, and unit of parameters shown in the mathematical models. The estimation values of the parameters are from the model fit of experimental data shown in Figure 2.2d,e,f

equilibrium above zero highly depend on these parameters. For example, the system goes through a saddle-node bifurcation when n decreases from 2.5 to 1.0, where the bifurcation occurs around 1.88. This means that if n is above 1.88, the system has two stable states

and can work as a bistable switch while the system is monostable if n is below 1.88 and cannot work as a bistable switch at all. The parameter n represents the Hill coefficient for ZAVNY, which indicates that changing the cooperative binding of ZAVNY will have an effect on the bistability. Similar saddle-node bifurcations also occur when changing parameters k_0 , k_2 , and k_4 . Parameters k_0 and k_2 together model the ZAVNY synthesis rate caused by the positive feedback of ZAVNY, where k_0 is positively correlated with the synthesis rate and k_2 is negatively correlated with the synthesis rate. Parameter k_4 models the dilution and degradation rate of ZAVNY. The analysis indicates that a suitable parameter range is critical to the bistability of the system. This also provides guidance on how to tune the switch. For example, to achieve a higher ON state equilibrium value, one may need to redesign ZAVNY to increase the positive feedback synthesis rate, decrease the degradation and dilution rate, or increase the cooperativity.

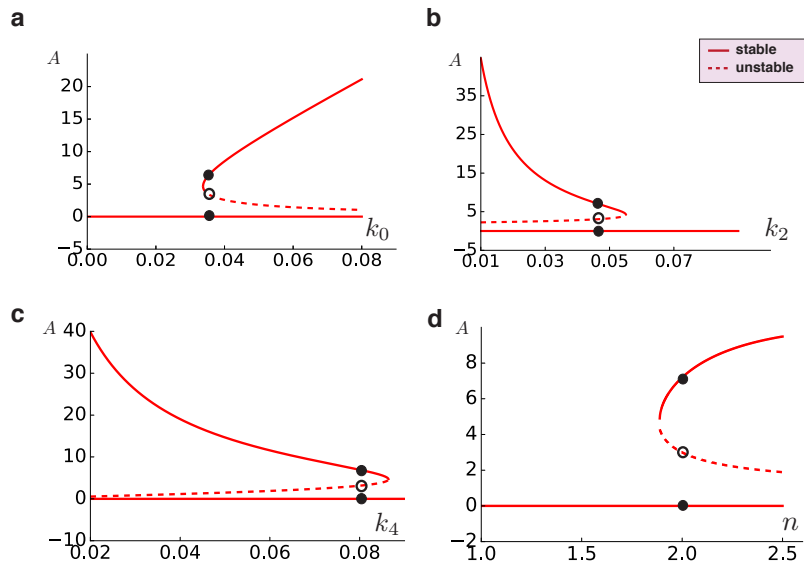


Figure 2.6: Bifurcation diagrams for the bistable switch system for parameters k_0 , k_2 , k_4 , and n . The dots and circles indicate the stable and unstable equilibria under the estimated parameter values.

2.4 Methods

2.4.1 Build Methods

All plasmids used in this chapter were listed in Appendix A Table A.1 with publicly available sequences linked in Benchling. They were constructed on ampicillin resistant backbone vector via Gibson assembly [21], amplified in *E. coli* DH5 α , extracted using QIAGEN miniprep kits, and sequence verified with Genewiz. All yeast strains used in this chapter were listed in Appendix A Table A.2 by their reference name in the chapter along with the plasmids that were integrated into their genome. The plasmids listed in each strain were digested by PmeI restriction enzyme from NEB to get linearized fragment and then sequentially integrated into the yeast genome using a standard lithium acetate yeast transformation protocol [22]. The base yeast strain used for the yeast transformation is MATa W303-1A, a gift from the Gottschling laboratory. All plasmids and yeast strains were constructed through the cloning processes in Aquarium, a software-enabled human-in-the-loop automation platform developed in the Klavins lab. Technicians in the University of Washington Biofabrication Center (UW BIOFAB), an Aquarium enabled cost center for providing molecular cloning services, carried out the lab procedures.

2.4.2 Test Methods

Media Preparation

Synthetic complete (SC) media were used as the base yeast media across the time-course cytometry assays. The input 00 was base yeast media, the input 10 was base media containing 100 nM β -e, and the input 01 was base media containing 20 μ M auxin. β -e was made from β -Estradiol dry stock, and auxin was made from 3-Indoleacetic acid dry stock, both ordered from Sigma-Aldrich.

Time-course Cytometry Assays

To prepare each assay, for each experimental strain, three freshly grown colonies on YPD plate were inoculated in SC media in a 96 deepwell plate, and then grew in 30 C shaker incubator for 12 hours. For the bistable switch strain, 20 μ M auxin were added in the media after inoculation, while other procedures kept the same. This was to prepare the bistable switch strain to be at OFF state at 0 h in the assay. After a 12-hour incubation, cytometry measurements were performed for each culture. Cell density was estimated using cytometry data gated for yeast singlets population by the self-developed Python package Cowfish. Each culture was then diluted to 1 event per μ L in its respective input media. Immediately after dilution, yeast cell measurements were performed over flow cytometer to obtain the 0 h data. Subsequent measurements were acquired every 6-12 hours according to the experimental charts (Figure 2.2d, e, f). Each culture was diluted to a constant cell density of 1 event per μ L in the respective input media when applying each input step.

Flow Cytometry

For each measurement, 100 μ L of each sample in the 96 deepwell plate was transferred to a Costar 96 well assay plate and placed on the BD Accuri C6 flow cytometer plate adapter. Yeast cell measurements including fluorescence, size, and count were obtained using excitation wavelengths of 488 and 640 nm and an emission detection filter at 533/30 nm (FL1 channel). A total of 10,000 events above a 400,000 FSC-H threshold (to exclude debris) were measured for each sample at a flow rate of 66 mL/min and core size of 22 mm using the Accuri C6 software. Data were exported as FCS 3.0 files and processed by self-developed Python package Cowfish.

2.5 Summary

In this chapter, we presented the design, construction, and validation of a synthetic bistable switch in yeast. The switch design is based on a positive feedback loop with a novel tran-

scriptional activator called ZAVNY. The design incorporated an extra activator, ZEV, which enabled turning the switch ON with β -e and an auxin receptor TIR1DM, which enabled turning the switch OFF with auxin. We experimentally built the bistable switch and tested its function using time course cytometry. The entire build and test process were carried out using Aquarium, a software enabled human-in-the-loop automation platform, which we will discuss in detail in Chapter 5. To elucidate the theoretical principles behind the bistable switch, we developed a simple mathematical model. The model was derived from a full mechanistic model of the reactions involved, and reduced to a one-dimensional model using mass conservation and quasi steady state assumptions. The model was used to fit the experimental data and perform bifurcation studies to illustrate changes in stability profile when different inputs were applied to the switch or certain parameters were tuned.

Chapter 3

DESIGN, CONSTRUCTION, AND VALIDATION OF A REWRITABLE ANTIBIOTIC RESISTANCE MEMORY IN YEAST

Synthetic bistable switches have been realized *E. coli* [20] and mammalian cells [34, 36]. However, little has been shown on how to use these switches to build downstream applications. In Chapter 2, we presented a novel synthetic bistable switch in yeast. Here, we show an application of the bistable switch, rewritable antibiotic resistance memory (ReARM). In this chapter, we describe the circuit design of the ReARM, which is realized by connecting the switch with a downstream antibiotic resistance gene. We implemented the design and experimentally demonstrated the functionality of ReARM by measuring its growth rate with different inputs. We developed a mathematical model of ReARM that included the bistable switch model in Chapter 2 and used the model to fit the experimental data.

3.1 Circuit Design

By connecting the bistable switch with a downstream antibiotic resistance gene, we developed a new circuit that works as rewritable antibiotic resistance memory (ReARM). The circuit diagram of ReARM (Figure 3.1a) shows that the new circuit is composed of the bistable switch and a pGALZ promoter driven BleoMX gene. BleoMX encodes for the bleomycin resistance protein. The expression of BleoMX confers resistance to the antibiotic Zeocin, which belongs to bleomycin family and is commonly used in molecular biology as a selection marker [17]. Theoretically, when the bistable switch is in the ON state, ZAVNY is at a high level driving the expression of BleoMX and the cells are resistant to Zeocin. When the bistable switch is in the OFF state, ZAVNY is absent and BleoMX is not expressed, thus

the cells are not resistant to Zeocin. Since the bistable switch can be switched between ON and OFF states repeatedly using β -e and auxin, we expect similar repeatable switchability of Zeocin resistance in the new circuit. The bistable switch is stable at either ON or OFF state without the continuing presence of inducers. Thus we expect the Zeocin resistance will also be stable. Therefore we expect the new circuit to be a rewritable antibiotic resistance memory that can be set ON or OFF repeatedly, while maintaining the ON or OFF state without the continuing presence of inducers.

3.2 Experimental Results

We performed time course plate reader assays to show the functionality of ReARM cells. SC media with $400 \mu\text{g/mL}$ Zeocin was used as the base yeast media for the assay. The input 00 was base yeast media, the input 10 was base media containing 100 nM β -e, and the input 01 was base media containing $20 \mu\text{M}$ auxin. ReARM cells were cycled through inputs 10, 00, 01, 00, and 10, as shown in Figure 3.1c. The observed growth rate was high when the switch was supposed to be ON, while the observed growth rate was low to undetectable when the switch was supposed to be OFF. This behavior is consistent with the hypothesis that once BleoMX reaches a low enough level, cell death induced by Zeocin outpaces cell growth. ReARM cells were able to remember a pulse of β -e for at least four subsequent dilution steps using input 00 (Figure 3.1d). In contrast, our control strain without the bistable switch circuitry, did not remember a pulse of β -e, and showed no growth within two steps after the removal of β -e (Figure 3.1f). Cells were not able to escape the OFF state in five steps (Figure 3.1e), showing that the OFF state was stable.

3.3 Mathematical Models

In this section, we developed mathematical models for the ReARM (Figure 3.2a) and the control strain without bistable switch (Figure 3.2b). First, we show the derivation of a model for describing the dynamics of ZAVNY and BleoMX from a full mechanistic model of the reactions involved reduced to a two-dimensional model using mass conservation and

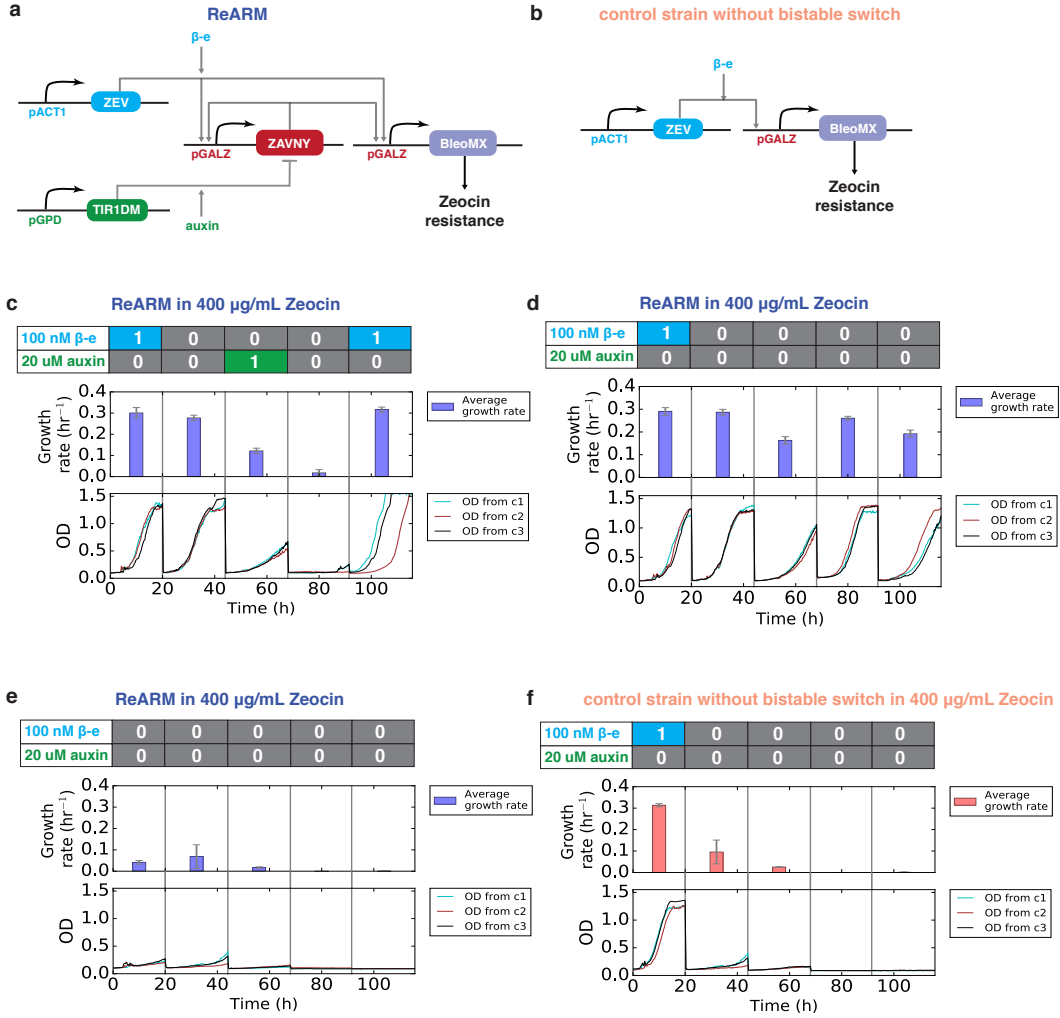


Figure 3.1: A rewritable antibiotic resistance memory (ReARM) in yeast. (a) Circuit diagram of the ReARM in yeast. (b) Circuit diagram of the control strain without the bistable switch circuitry. (c, d, e, f) Growth rate and growth curve of ReARM and the control strain without bistable switch under series of inputs. (c) Experimental data showed the switchability of the resistance memory. Cells were grown in 400 $\mu\text{g/mL}$ Zeocin media plus respective inducers determined by the inputs. Growth rate was high with input 10, kept high with input 00, changed to low with input 01, kept low with input 00, and changed to back to high with input 10. (d) Experimental data showed ON state stability of the resistance memory. Growth rate kept high after input 10 with at least four steps of 00. (e) Experimental data demonstrating the OFF state stability of the resistance memory, noting that the strains were induced with 20 μM auxin to switch to OFF state before 0 h. (f) Experimental data showed that control strain without bistable switch did hold ON state. The growth rate dropped from high to low after input 10 was changed to input 00 at 20 h.

quasi steady state assumptions (Figure 3.3). Then we developed rate equations that describe the dynamics of population and nutrients based on Monod equation. By combining these equations, we got a 4D ODE model that describes the dynamics of ZAVNY, BleoMX, population size, and nutrient concentration. We use the model to predict ZAVNY and BleoMX concentration dynamics and fit the growth curve in the experiments.

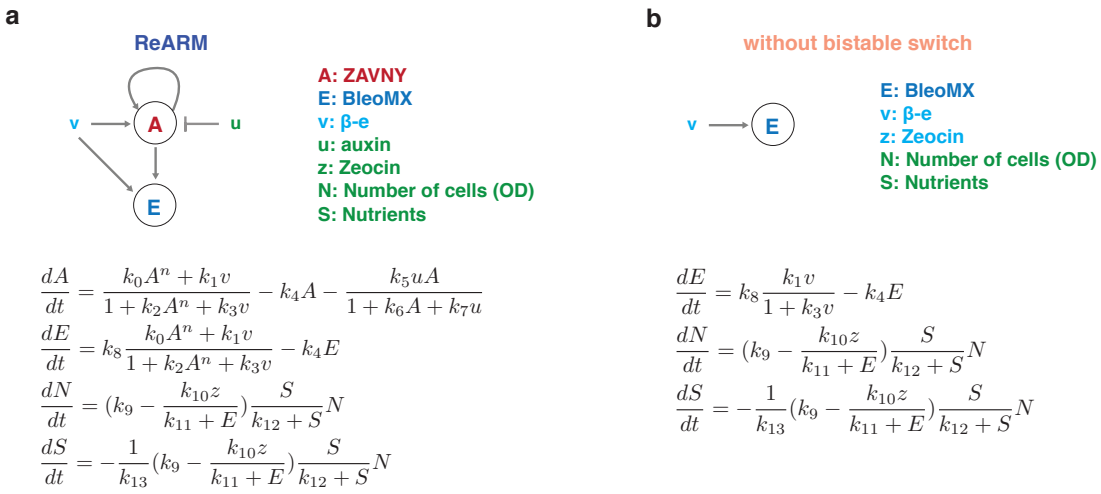


Figure 3.2: Simplified circuit diagram and mathematical models of two experimental yeast strains (a) ReARM, and (b) the control strain without the bistable switch.

3.3.1 Model Derivation

ReARM

The ReARM circuit can be modeled through the biochemical reaction network shown in Figure 3.3, where we drew a schematic network of how genes and proteins interact in this biochemical circuit and gave their corresponding chemical equations. We did not specifically model the mRNA in this network, the parameters $\alpha_{aa}, \alpha_{ab}, \alpha_{ea}, \alpha_{eb}\alpha_b, \alpha_f$ are lumped parameters that describe the net effect of transcription and translation. All the rate parameters are positive real numbers. Assuming mass action kinetics, the temporal dynamics of this

system are given by the reaction rate equations as

$$\begin{aligned}
\frac{dG_a}{dt} &= \theta_{aa}G_{aa} + \theta_{ab}G_{ab} - \gamma_{aa}G_aA - \gamma_{ab}G_aB^* \\
\frac{dG_{aa}}{dt} &= \gamma_{aa}G_aA - \theta_{aa}G_{aa} \\
\frac{dG_{ab}}{dt} &= \gamma_{ab}G_aB^* - \theta_{ab}G_{ab} \\
\frac{dG_e}{dt} &= \theta_{ea}G_{ea} + \theta_{eb}G_{eb} - \gamma_{ea}G_eA - \gamma_{eb}G_eB^* \\
\frac{dG_{ea}}{dt} &= \gamma_{ea}G_eA - \theta_{ea}G_{ea} \\
\frac{dG_{eb}}{dt} &= \gamma_{eb}G_eB^* - \theta_{eb}G_{eb} \\
\frac{dA}{dt} &= -\gamma_{aa}G_aA + \theta_{aa}G_{aa} - \gamma_{ea}G_eA + \theta_{ea}G_{ea} + \alpha_{aa}G_{aa} + \alpha_{ab}G_{ab} - \gamma_{af}AF^* - \delta_aA \quad (3.1) \\
\frac{dB}{dt} &= \alpha_bG_b - \delta_bB \\
\frac{dB^*}{dt} &= -\gamma_{ab}G_aB^* + \theta_{ab}G_{ab} - \gamma_{eb}G_eB^* + \theta_{eb}G_{eb} + \omega_bvB - \delta_bB^* \\
\frac{dF}{dt} &= \alpha_fG_f + \delta_{af}A_f - \omega_fuF - \delta_fF \\
\frac{dF^*}{dt} &= \omega_fuF - \gamma_{af}AF^* - \delta_fF^* \\
\frac{dA_f}{dt} &= \gamma_{af}AF^* - \delta_{af}A_f \\
\frac{dE}{dt} &= \alpha_{ea}G_{ea} + \alpha_{eb}G_{eb} - \delta_eE,
\end{aligned}$$

where $G_a, G_{aa}, G_{ab}, G_e, G_{ea}, G_{eb}, A, B, E, F, B^*, F^*$, and A_f represent the concentrations of these species shown in Figure 3.3. They are consistent with what were shown in Figure 2.3.

Assuming quasi-steady-state for all species other than A and E , we can set corresponding rate equations to be zero. It's also reasonable to assume that the binding and unbinding rates for G_e and G_a are the same since they have the same promoter pGAL1. Thus we can set $\theta_{ea} = \theta_{ea}$, $\gamma_{ea} = \gamma_{ea}$, $\theta_{eb} = \theta_{eb}$, and $\gamma_{eb} = \gamma_{eb}$. Without loss of generality, we assume that the total gene copy for E is 1 as we assume the total gene copy for A is also 1. We have

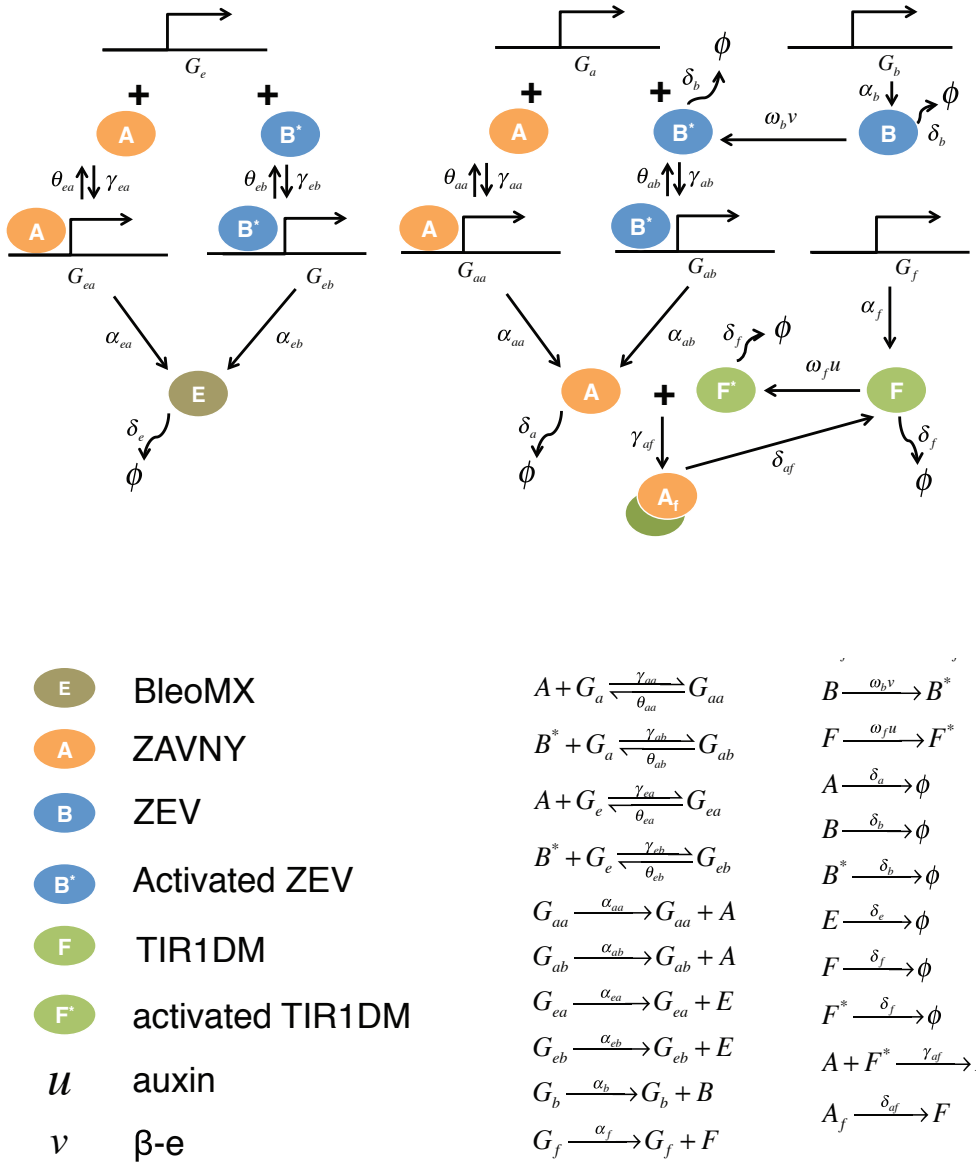


Figure 3.3: Biochemical reaction network of the ReARM. A is ZAVNY, B is ZEV, F is TIR1DM, E is BleoMX, B^* is ZEV bound by β -estradiol, and F^* is the TIR1DM bound by auxin. Additional to what described in Figure 2.3, G_e is E's coding gene that not being activated. G_{ea} and G_{eb} are G_e that being bound by A and B^* , which are activated and can be transcribed and translated to A with different rates α_{ea} and α_{eb} . The rest of the interactions and rate parameters are self-explanatory by inspection of the graph.

$G_e + G_e a + G_e b = 1$. After mathematical derivation, we get the dynamics for A and R as

$$\begin{aligned}\frac{dA}{dt} &= \frac{\lambda_a A + \lambda_b \pi_b v}{1 + \rho_a A + \rho_b \pi_b v} - \frac{\lambda_f \gamma_{af} A u}{\delta_f + \gamma_{af} A + \omega_f u} - \delta_a A \\ \frac{dE}{dt} &= \frac{\lambda_{ea} A + \lambda_{eb} \pi_b v}{1 + \rho_a A + \rho_b \pi_b v} - \delta_e E,\end{aligned}\quad (3.2)$$

where $\lambda_a = \frac{\gamma_{aa}}{\theta_{aa}} \alpha_{aa}$, $\lambda_b = \frac{\gamma_{ab}}{\theta_{ab}} \alpha_{ab}$, $\lambda_{ra} = \frac{\gamma_{aa}}{\theta_{aa}} \alpha_{aa}$, $\lambda_{rb} = \frac{\gamma_{ab}}{\theta_{ab}} \alpha_{ab}$, $\rho_a = \frac{\gamma_{aa}}{\theta_{aa}}$, $\rho_b = \frac{\gamma_{ab}}{\theta_{ab}}$, $\pi_b = \frac{\omega_b}{\delta_b^2} \alpha_b$, and $\lambda_f = \frac{\omega_f \alpha_f}{\delta_f}$. We then generalize Equation 3.2 as follows to model the cooperativity of ZAVNY in DNA binding:

$$\begin{aligned}\frac{dA}{dt} &= \frac{\lambda_a A^n + \lambda_b \pi_b v}{1 + \rho_a A^n + \rho_b \pi_b v} - \frac{\lambda_f \gamma_{af} A u}{\delta_f + \gamma_{af} A + \gamma_{rf} R + \omega_f u} - \delta_a A \\ \frac{dE}{dt} &= \frac{\lambda_{ea} A + \lambda_{eb} \pi_b v}{1 + \rho_a A + \rho_b \pi_b v} - \delta_e E,\end{aligned}\quad (3.3)$$

where n is the Hill coefficient and $n > 0$.

By renaming parameters as k_0 to k_n for easier communication, we have the following:

$$\begin{aligned}\frac{dA}{dt} &= \frac{k_0 A^n + k_1 v}{1 + k_2 A^n + k_3 v} - k_4 A - \frac{k_5 a A}{1 + k_6 A + k_7 u} \\ \frac{dE}{dt} &= k_8 \frac{k_0 A^n + k_1 v}{1 + k_2 A^n + k_3 v} - k_4 E.\end{aligned}\quad (3.4)$$

Adding rate equations for population and nutrients, we get the following:

$$\begin{aligned}\frac{dA}{dt} &= \frac{k_0 A^n + k_1 v}{1 + k_2 A^n + k_3 v} - k_4 A - \frac{k_5 a A}{1 + k_6 A + k_7 u} \\ \frac{dE}{dt} &= k_8 \frac{k_0 A^n + k_1 v}{1 + k_2 A^n + k_3 v} - k_4 E \\ \frac{dN}{dt} &= (k_9 - \frac{k_{10} z}{k_{11} + E}) \frac{S}{k_{12} + S} N \\ \frac{dS}{dt} &= -\frac{1}{k_{13}} (k_9 - \frac{k_{10} z}{k_{11} + E}) \frac{S}{k_{12} + S} N.\end{aligned}\quad (3.5)$$

Control without the Bistable Switch

The control strain, lacking ZAVNY (A), is modeled with the following equations.

$$\begin{aligned}\frac{dE}{dt} &= k_8 \frac{k_1 v}{1 + k_3 v} - k_4 E \\ \frac{dN}{dt} &= (k_9 - \frac{k_{10} z}{k_{11} + E}) \frac{S}{k_{12} + S} N \\ \frac{dS}{dt} &= -\frac{1}{k_{13}} (k_9 - \frac{k_{10} z}{k_{11} + E}) \frac{S}{k_{12} + S} N.\end{aligned}\tag{3.6}$$

3.3.2 Model Fit

Growth curves with OD data from 3 replicates were fit to these ODEs using the downhill simplex algorithm with customized Python code with 8 parameters determined by the model's fit to the bistable switch experimental data. The model fits are shown as red lines (Figure 3.2). The fitting parameter values are listed (Table 3.1) along with parameter descriptions and units. Model predicted ZAVNY and BleoMX concentration dynamics are shown as solid lines in the middle portion of the subfigures (Figure 3.2).

3.4 Methods

3.4.1 Build Methods

Build methods for ReARM and its control are exactly the same as the bistable switch strain and its controls. Refer to Chapter 2 Build and Test Methods section.

3.4.2 Test Methods

Media Preparation

Synthetic complete (SC) media with 400 $\mu\text{g}/\text{mL}$ were used as the base yeast media across the plate reader assays. The input 00 was base yeast media, the input 10 was base media containing 100 nM β -e, and the input 01 was base media containing 20 μM auxin. β -e was

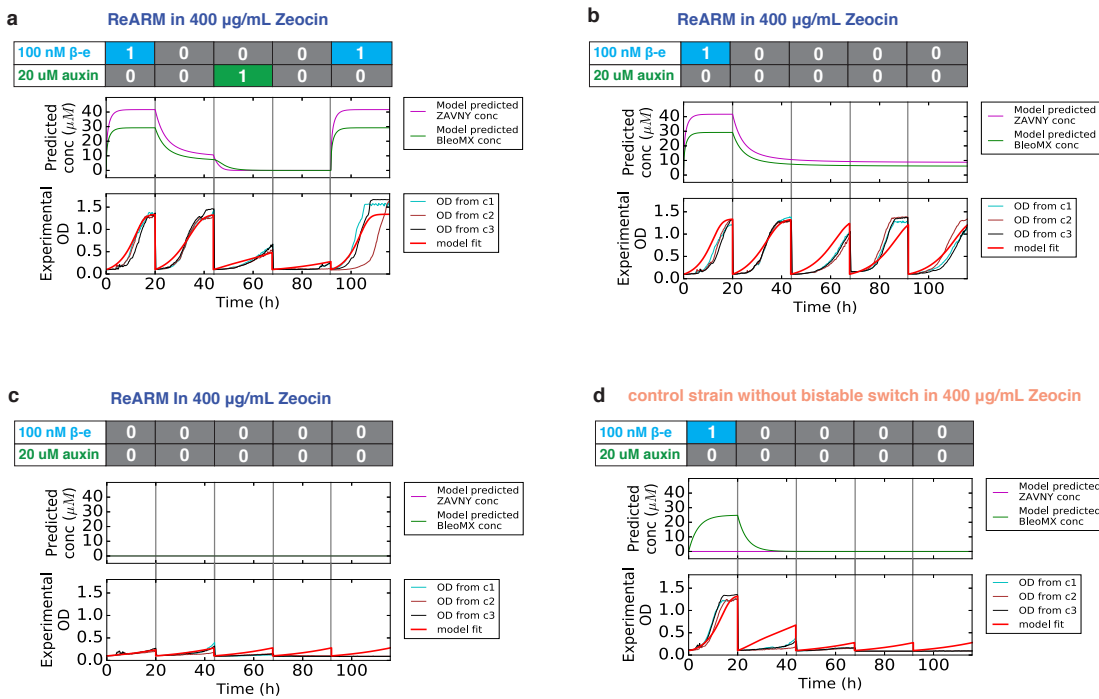


Figure 3.4: Model prediction and growth curve fitting for the time course plate reader assay. Red line in each figure shows the model fit with parameters estimations shown in Table 3.1. Model predicted ZAVNY and BleoMX concentration dynamics are shown in the upper portion of each subplot.

Parameter	Description	Estimation	Units
k_8	Difference in synthesis rate between ZAVNY and BleoMX	0.701	Unitless
k_9	Maximum growth rate without the presence of Zeocin	0.361	h^{-1}
k_{10}	Parameter controlling the maximum growth rate reduction due to Zeocin	7.51	μM
k_{11}	Half-saturation constant of BleoMX	10.01	h^{-1}
k_{12}	Half-saturation constant of the nutrients	4.011	g/L
k_{13}	Growth yield	0.124	Unitless

Table 3.1: Description, estimation, and unit of parameters shown in the mathematical models. The estimation values of the parameters are from the model fit of experimental data shown in Figure 3.4

made from β -Estradiol dry stock, and auxin was made from 3-Indoleacetic acid dry stock, both ordered from Sigma-Aldrich.

Time-course Plate Reader Assays

The preparation step is similar to the time-course cytometry assays. Three freshly grown colonies from YPD plate for each strain were inoculated in SC media in a 96 deepwell plate, and then grew in 30 C shaker incubator for 12 hours. For the ReARM strain, 20 μM auxin were added in the media after inoculation to make sure the switch was switched to OFF state. After 12-hour incubation, cell density was estimated using cytometry data gated for yeast singlets population by the Python package Cowfish. Yeast culture was then diluted to 1 event per μL in 1 mL of respective input media in a VWR 24-well tissue culture plate. The plate was placed in a Bioteck Synergy HT plate reader at 30 C with shaking and measured every 15 minutes. Yeast culture was diluted every 20-24 h to a constant cell density of 1

event per μL in the respective input media according to the experimental chart (Figure 3.1c, d, e, f).

Plate Reader Measurements

Yeast cells were cultured in a VWR 24-well tissue culture plate with lid covered in a Biotek Synergy HT plate reader at 30 C with shaking. Cell culture optical densities (OD, 600 nm) were taken every 15 minutes through scheduling from the Gen5 software. Data were exported as tab-delimited text file and processed by custom Python scripts to fit exponential growth curve and calculate growth rate.

3.5 Summary

In this chapter, we presented the design, construction, and validation of rewritable antibiotic resistance memory (ReARM). ReARM was designed and built as an application of the novel bistable switch we presented in Chapter 2. ZAVNY in the bistable switch was used to drive the expression of the Zeocin resistance gene, BleoMX. Time course plate reader assays with a series of inputs were carried out to demonstrate the switchability and long term stability of ReARM. We developed a mathematical model for the ReARM that included the bistable switch model, and also included equations for the rates of change of the BleoMX protein, the population size, and the nutrient concentration. We used the model to fit the growth curve data and predicted the dynamics of ZAVNY and BleoMX. The model and predictions illustrate the mechanism that ZAVNY drives BleoMX and BleoMX promotes growth in the ReARM circuit.

Chapter 4

DESIGN, ANALYSIS, AND HIGH-THROUGHPUT TESTING METHOD OF AN AUXIN-SENSITIVE RELAXATION OSCILLATOR IN YEAST

4.1 *Introduction*

Oscillators are at the heart of cell physiology. Cells grow and divide periodically, governed by oscillators [45]. Many metabolic processes show oscillations, such as glycolysis in anaerobic yeast cells [27]. Circadian rhythms are biological oscillatory processes, with 24 hour cycles, found across all domains of life [33, 44, 56]. Since the discovery of oscillatory phenomena in cells, researchers have been trying to understand how various oscillators work in biological systems. Over the past decade researchers have built synthetic oscillators for various applications in multiple organisms including *E. coli* [7, 13, 16, 53] and mammalian cells [55]. However, a truly robust, tunable, and modular oscillator technology has not been demonstrated in eukaryotic cells. In this chapter, we describe a design for an auxin-sensitive relaxation oscillator (ASRO) in yeast, specifically *S. cerevisiae*, and give a detailed theoretical analysis.

4.2 *ASRO design*

The ARSO uses the classical activation-repression relaxation architecture [24], similar to the well known Hasty oscillator [53]. In contrast to Hasty oscillator, the repressing element operates post-translationally rather than the transcriptional level. The circuit design is shown in Figure 4.1.a. The circuit consists of two components: an auxin-sensitive transcription activator (ASTA) and an F-Box protein (FBox). ASTA activates the synthesis of both itself and FBox through transcriptional activation. The FBox represses ASTAs function via protein degradation mediated by the plant hormone auxin *auxin*. A design for the ASTA

is proposed in Figure 4.1.b, where domain II is an auxin degron. The auxin degron causes the chimeric protein to be ubiquitinated by the FBox in the presence of auxin. This process has been well characterized in yeast [26, 31, 43]. The transcription activator ZAVNY in the bistable switch presented in Chapter 2 is an instance of ASTA.

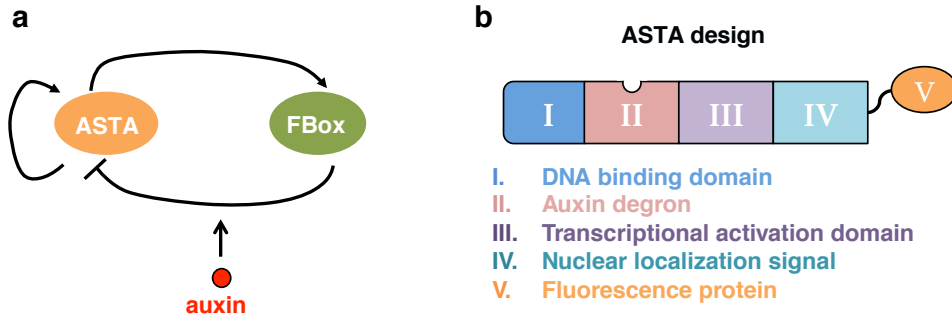


Figure 4.1: The ASRO design (a) Circuit diagram of the auxin-sensitive relaxation oscillator (ASRO), where ASTA is an auxin-sensitive transcription activator and FBox is an F-Box protein. ASTA activates the synthesis of both ASTA and FBox, while FBox degrades ASTA in the presence of the plant hormone auxin. (b) ASTA schematic design consists of four protein domains and a fused fluorescence protein. Domain I, II, IV together realize the transcriptional activating function of the chimeric protein. Domain II is an auxin degron, which makes the protein subject to auxin induced degradation by FBox.

4.3 Mathematical Models

ASRO circuit can be modeled through the biochemical reaction network shown in Figure 4.2. This network encompass all the interactions between the promoters, mRNAs and proteins in the system. Chemical equations of all interactions are written out and all the rate parameters are positive real numbers.

Assuming mass action kinetics, the temporal dynamics of this system are given by the following reaction rate equations shown in Equation 4.1, where $G_A, G_F, M_A, M_F, A, F, C$ represent the concentrations of these species as explained in Figure 4.2. A similar approach has been used in modeling biochemical oscillators [57]. This model holds under the assumptions that all the reactions happen in a well mixed macroscopic reactor such as a continuous

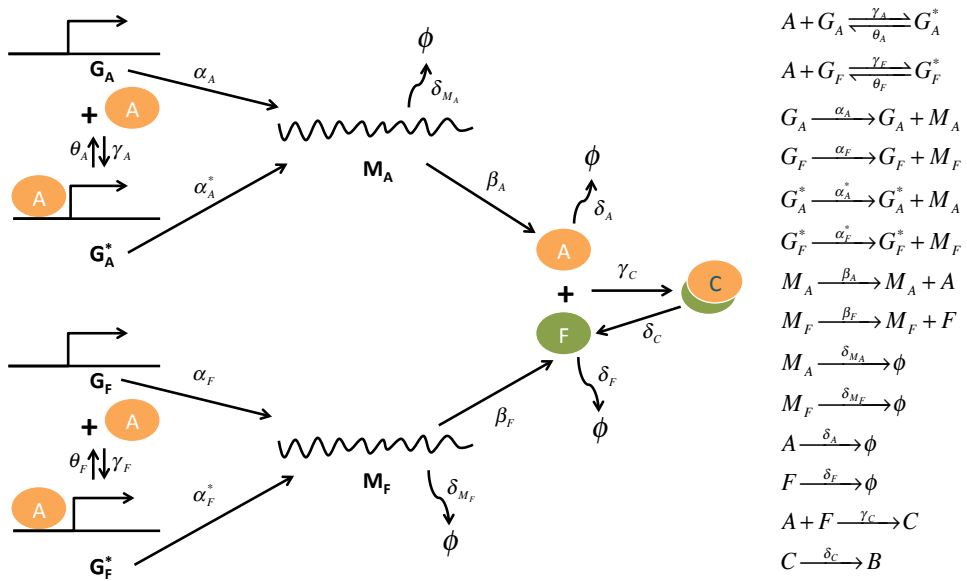


Figure 4.2: Biochemical reaction network of the ASRO. A is short for ASTA and F is short for FBox for simple illustrations. G_A and G_F are genes coding for A and F that are not activated by A, while G_A^* and G_F^* are genes that are activated by A. M_A and M_F are mRNAs that code for A and F. C is the protein complex formed by A and F through protein interactions induced by auxin. A is targeted by ubiquitin for protein degradation in the complex C hence $C \xrightarrow{\delta_C} F$. Rate parameters in this biochemical reaction network are self-explanatory by inspection of the graph. We assume that the transcription rates caused by activator A is greater than the leaky expression, thus having $\alpha_A > \alpha_A^*$ and $\alpha_F > \alpha_F^*$. Also noting that rate γ_C is dependent on auxin concentration.

culture device [54].

$$\begin{aligned}
\frac{dG_A}{dt} &= \theta_A G_A^* - \gamma_A G_A A \\
\frac{dG_F}{dt} &= \theta_F G_F^* - \gamma_F G_F A \\
\frac{dM_A}{dt} &= \alpha_A G_A + \alpha_A^* G_A^* - \delta_{M_A} M_A \\
\frac{dM_F}{dt} &= \alpha_F G_F + \alpha_F^* G_F^* - \delta_{M_F} M_F \\
\frac{dA}{dt} &= \beta_A M_A + \theta_A G_A^* + \theta_F G_F^* - \gamma_A G_A A - \gamma_F G_F A - \gamma_C A F - \delta_A A \\
\frac{dF}{dt} &= \beta_F M_F - \gamma_C A F + \delta_C C - \delta_F F \\
\frac{dC}{dt} &= \gamma_C A F - \delta_C C.
\end{aligned} \tag{4.1}$$

In this circuit, the dynamics of genes, mRNAs, and protein interaction and ubiquitination are faster than the synthesis and dilution of the proteins. Therefore we can make quasi-steady-state assumptions on G_A, G_F, M_A, M_F, C , hence setting corresponding rate equations to be zero. Through simplification, we get the two-dimensional system shown in Equation 4.2.

$$\begin{aligned}
\frac{dA}{dt} &= \frac{\lambda_A + \pi_A \rho_A A}{1 + \rho_A A} - \gamma_C A F - \delta_A A \\
\frac{dF}{dt} &= \frac{\lambda_F + \pi_F \rho_F A}{1 + \rho_F A} - \delta_F F,
\end{aligned} \tag{4.2}$$

where $\lambda_A = \frac{\beta_A}{\delta_{M_A}} \alpha_A$, $\lambda_F = \frac{\beta_F}{\delta_{M_F}} \alpha_F$, $\pi_A = \frac{\beta_A}{\delta_{M_A}} \alpha_A^*$, $\pi_F = \frac{\beta_F}{\delta_{M_F}} \alpha_F^*$, $\rho_A = \frac{\gamma_A}{\theta_A}$, and $\rho_F = \frac{\gamma_F}{\theta_F}$. Also since we know that $\alpha_A > \alpha_A^*$ and $\alpha_F > \alpha_F^*$, it follows that $\pi_A > \lambda_A$ and $\pi_F > \lambda_F$, which will be useful in later theoretical analysis.

Equation 4.2 can be rewritten as

$$\begin{aligned}
\frac{dA}{dt} &= f_1(A) - \gamma_C A F - \delta_A A \\
\frac{dF}{dt} &= f_2(A) - \delta_F F,
\end{aligned} \tag{4.3}$$

where $f_1(A)$ and $f_2(A)$ are defined by

$$f_1(A) = \frac{\lambda_A + \pi_A \rho_A A}{1 + \rho_A A}, f_2(A) = \frac{\lambda_F + \pi_F \rho_F A}{1 + \rho_F A}. \quad (4.4)$$

Essentially $f_1(A)$ and $f_2(A)$ are Hill functions with Hill coefficient $n = 1$. More generally, we can let $f_1(A)$ and $f_2(A)$ be general Hill functions [50] as

$$f_1(A) = \frac{\lambda_A + \pi_A \rho_A A^n}{1 + \rho_A A^n}, f_2(A) = \frac{\lambda_F + \pi_F \rho_F A^n}{1 + \rho_F A^n}, \quad (4.5)$$

where n is the Hill coefficient and $n > 0$. This general Hill function makes our model more valid as it takes ASTA's cooperativity into account.

4.4 Requirements for Sustained Oscillations

Considering the two-component oscillator modeled by Equations 4.3 with general Hill function defined by Equations 4.5, let's call this oscillator model as S . S is essentially a two-dimensional nonlinear dynamical system. The Poincaré-Bendixson theorem informs us that the system has periodic solutions if it is confined in a bounded region that does not contain any stable fixed points.

4.4.1 Sustained Oscillations Requirements Based on the Poincaré-Bendixson Theorem

Assume that the system has a unique equilibrium point (A^*, F^*) on \mathbb{R}_+^2 . Conditions for having a single equilibrium point can be deduced in similar fashion as found in [14]. First we show that the system is confined in a bounded region on the phase plane, which is equivalent to showing that the system is operating on a positively invariant set.

Lemma 1. *There exist constants $D_1, D_2 \in \mathbb{R}_+$ such that the set $K = \{(A, F) \in \mathbb{R}_+^2 | A \leq D_1, F \leq D_2\}$ is positively invariant under the vector field defined by system S .*

Proof. By definition, both $f_1(A)$ and $f_2(A)$ are positive bounded functions. K is defined by 4 boundaries $A = 0, F = 0, A = D_1, F = D_2$ on \mathbb{R}_+^2 . We can show that on each

boundary, the vector defined by system S is pointing inward to the set K . For $A = 0$, we have $dA/dt = f_1(A) > 0$. For $F = 0$, we have $df/dt = f_2(A) > 0$. Therefore all the vectors on boundary $A = 0$ and $F = 0$ are pointing inward to the set as shown in Figure 4.3.a. For boundary $A = D_1$, let $M_1 = \sup\{f_1(A)|A \in R^+\}$, we have $dA/dt = f_1(D_1) - \gamma_c D_1 F - \delta_A D_1 < M_1 - \delta_A D_1$. By choosing $D_1 = \max\{M_1/\delta_A, A^*\}$, we have $dA/dt < M_1 - \delta_A D_1 = 0$, thus vectors on this boundary point inward. Similarly, for boundary $F = D_2$, let $M_2 = \sup\{f_2(A)|A \in R^+\}$, we have $df/dt = f_2(A) - \delta_F D_2 < M_2 - \delta_F D_2$. By choosing $D_2 = \max\{M_2/\delta_F, F^*\}$, we have $df/dt < M_2 - \delta_F D_2 = 0$, thus the vector on this boundary points inward as shown in Figure 4.3.a. Hence we know that K is a positively invariant set. Noting that by choosing $D_1 = \max\{M_1/\delta_A, A^*\}$ and $D_2 = \max\{M_2/\delta_F, F^*\}$, we also guarantee that $(A^*, F^*) \in K$. \square

Second, we derive the conditions for which system S contains no stable fixed points. The Jacobian matrix of system S at equilibrium (A^*, F^*) is

$$J(A^*, F^*) = \begin{pmatrix} \frac{\partial f_1(A^*)}{\partial A} - \gamma_C F^* - \sigma_A & -\gamma_C A^* \\ \frac{\partial f_2(A^*)}{\partial A} & -\delta_F \end{pmatrix}.$$

Sufficient conditions for the equilibrium to be unstable, i.e. real parts of the eigenvalues are all positive, are $\text{trace}(J(A^*, F^*)) > 0$ and $\det(J(A^*, F^*)) > 0$, which are guaranteed by following conditions.

$$(i) \quad \delta_F < \frac{(A^*)^{-1+n} n \rho_A (\pi_A - \lambda_A)}{(1 + \rho_A (A^*)^n)^2} - \gamma_C F^* - \delta_A$$

$$(ii) \quad \frac{(A^*)^{-1+n} n \rho_A (\pi_A - \lambda_A)}{(1 + \rho_A (A^*)^n)^2} - \gamma_C F^* - \delta_A < \frac{\gamma_C A^*}{\delta_F} \frac{(A^*)^{-1+n} n \rho_F (\pi_F - \lambda_F)}{(1 + \rho_F (A^*)^n)^2}$$

Theorem 1. *If system S has a single equilibrium (A^*, F^*) on \mathbb{R}_+^2 and it satisfies conditions (i) and (ii), S exhibits sustained oscillations.*

Proof. From Lemma 1 we know that the system is confined in a bounded region K where

$(A^*, F^*) \in K$. Conditions (i) and (ii) guarantee that this equilibrium point is either an unstable node or a spiral. It follows from the Poincaré-Bendixson theorem that for any initial condition $(A_0, F_0) \in K - \{(A^*, F^*)\}$, the system will either stay on a limit cycle or converge to a limit cycle, thus exhibiting sustained oscillations. \square

We now move on to explore for what parameters conditions (i) and (ii) are satisfied.

4.4.2 Hill Coefficient Requirements for Sustained Oscillations

In the following, we analyze how the Hill coefficient affects the existence of sustained oscillations for the system and derive a necessary condition on the Hill coefficient for sustained oscillations. Let $f(A, F) = f_1(A) - \gamma_C A F - \delta_A A$ and $g(A, F) = f_2(A) - \delta_F F$. Then two nullclines n_1 and n_2 of system S can be written as

$$\begin{aligned} n_1 : f(A, F) = 0 &\Rightarrow F = \frac{f_1(A)}{\gamma_C A} - \frac{\delta_A}{\gamma_C} = \frac{\lambda_A + \pi_A \rho_A A^n}{\gamma_C A (1 + \rho_A A^n)} - \frac{\delta_A}{\gamma_C} \\ n_2 : g(A, F) = 0 &\Rightarrow F = \frac{f_2(A)}{\delta_F} = \frac{\lambda_F + \pi_F \rho_F A^n}{\delta_F (1 + \rho_F A^n)} \end{aligned}$$

The derivatives of n_1 and n_2 are as follows

$$\begin{aligned} \frac{dF}{dA} \Big|_{f(A,F)=0} &= \frac{((n-1)\rho_a \pi_a A^n - \lambda_a)(1 + \rho_a A^n) - n A^n \rho_a (\lambda_a + A^n \rho_a \pi_a)}{A^2 \gamma_C (1 + \rho_a A^n)^2} \\ \frac{dF}{dA} \Big|_{g(A,F)=0} &= \frac{A^{-1+n} n \rho_F (\pi_F - \lambda_F)}{\delta_F (1 + \rho_F A^n)^2} \end{aligned}$$

We know that $\pi_F > \lambda_F$, therefore $\frac{dF}{dA} \Big|_{g(A,F)=0} > 0$.

Note that the Jacobian of system S can now be abstracted as

$$J(A, F) = \begin{pmatrix} \frac{\partial f}{\partial A} & \frac{\partial f}{\partial F} \\ \frac{\partial g}{\partial A} & \frac{\partial g}{\partial F} \end{pmatrix}.$$

Proposition 1. Any equilibrium satisfying $\frac{dF}{dA} \Big|_{f(A,F)=0} < 0$ is a stable fixed point.

Proof. Applying the implicit function theorem, we know that $\frac{dF}{dA} \Big|_{f(A,F)=0} = -\frac{\partial f / \partial A}{\partial f / \partial F} < 0$.

Since $\frac{\partial f}{\partial F} = -\gamma_C A < 0$, it follows that $\frac{\partial f}{\partial A} < 0$. Noting that $\frac{\partial g}{\partial F} = -\delta_F < 0$, therefore $\text{trace}(J) = \frac{\partial f}{\partial A} + \frac{\partial g}{\partial F} < 0$. Similarly, we have $\frac{dF}{dA}|_{g(A,F)=0} = -\frac{\partial g/\partial A}{\partial g/\partial F} > 0$. Since $\frac{\partial g}{\partial F} = -\delta_F < 0$, it follows that $\frac{\partial g}{\partial A} > 0$. Therefore $\det(J) = \frac{\partial f}{\partial A} \frac{\partial g}{\partial F} - \frac{\partial f}{\partial F} \frac{\partial g}{\partial A} > 0$. Hence the equilibrium is a stable fixed point. \square

Lemma 2. *Hill coefficient $n > 1$ is a necessary condition for system S to exhibit sustained oscillations.*

Proof. When Hill coefficient $n \leq 1$, it follows that

$$\frac{dF}{dA}|_{f(A,F)=0} \leq \frac{-\lambda_a(1 + \rho_a A^n) - n A^n \rho_a (\lambda_a + A^n \rho_a \pi_a)}{A^2 \gamma_C (1 + \rho_a A^n)^2} < 0$$

We know that $\frac{dF}{dA}|_{g(A,F)=0} > 0$. As shown in Figure 4.3.b, the two nullclines have only one intersection. This means that there exists only one equilibrium point for the system. Applying Proposition 1, we know that this equilibrium is a stable fixed point. Hence we know that Hill coefficient $n > 1$ is a necessary condition for the system to contain no stable fixed points, thus a necessary condition for the system to exhibit sustained oscillations. \square

Figure 4.3.c and Figure 4.3.d show numerical simulations of system S under the Hill coefficient values $n = 1$ and $n = 2$, while all other parameters are held the same. When $n = 1$, system S is stable while increasing n to 2 makes the system evolve towards a limit cycle, exhibiting sustained oscillations. Biochemically speaking, this means that we need to tune the activator A to have positive cooperative binding to the promoter. This could be achieved through modifying the DNA binding domain of A or the corresponding binding sites in the promoter [23].

4.4.3 Parameter dependent sustained oscillations analysis

In this section, we study how perturbations of the parameters related to DNA binding affinity and to auxin degradation strength, affect sustained oscillations. We know from Equation 4.2 and its derivation, that $\rho_A = \frac{\gamma_A}{\theta_A}$ and $\rho_F = \frac{\gamma_F}{\theta_F}$ represent the DNA binding affinity of

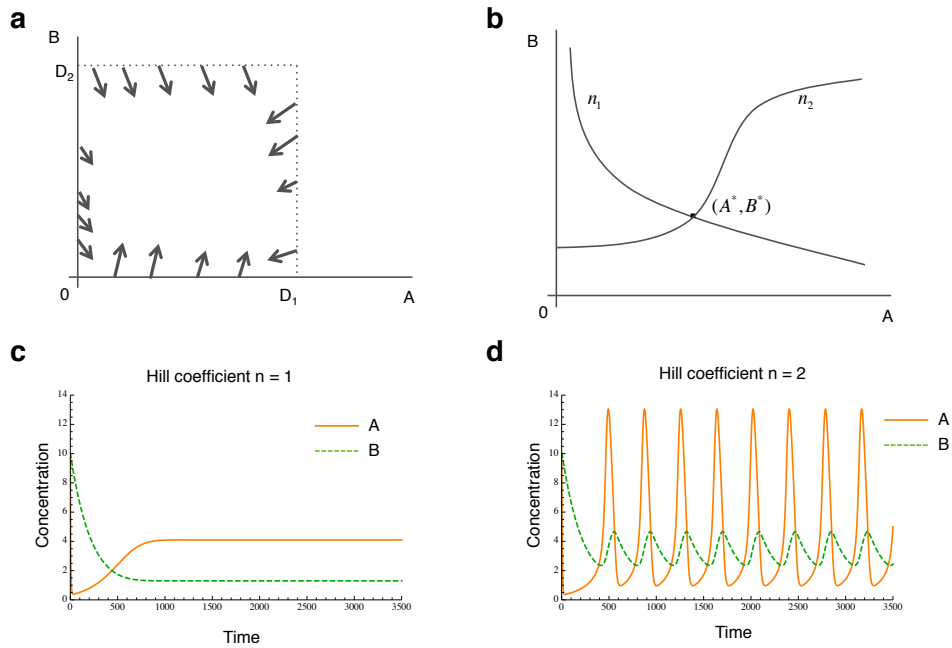


Figure 4.3: Sustained oscillations requirements analysis. (a) A simple phase plane graph on the Poincaré-Bendixson boundaries to explain that the system is confined in a bounded region. (b) Graphical illustration shows that the system has a single equilibrium when Hill coefficient $n = 1$. (c) Numerical simulations show that the system is non-oscillatory when $n = 1$. (d)) Numerical simulations produce sustained oscillations when Hill coefficient $n = 2$. The other parameters used in the two simulations are $\lambda_A = 0.08$, $\pi_A = 1.9$, $\rho_A = 0.01$, $\lambda_F = 0.002$, $\pi_F = 0.058$, $\rho_F = 0.01$, $\gamma_C = 0.025$, and $\delta_A = \delta_F = 0.0045$. These parameters are randomly chosen within a sensible biophysical range.

A to the promoters of G_A and G_F . Assuming that G_A and G_F are two instances of the same promoter within the cell, it is reasonable to have $\rho_A = \rho_F = \rho$. Hence, ρ represents the DNA binding affinity in the ASRO. Figure 4.4 shows how changing the value of ρ tunes the dynamical behavior of system S . We obtain similar results by perturbing parameter γ_C , which represents the auxin degradation strength in the ASRO.

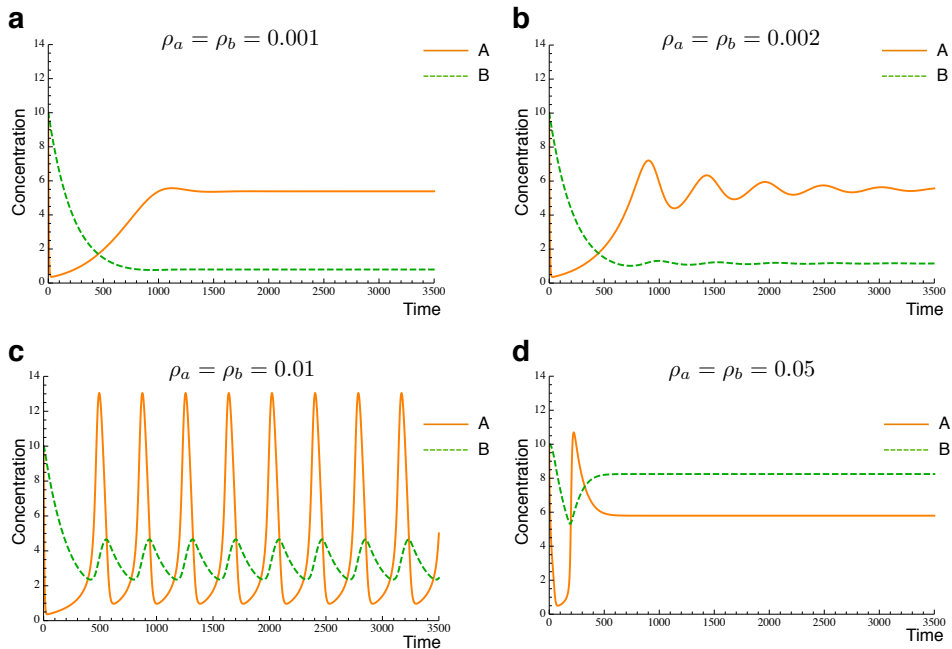


Figure 4.4: Changing the DNA binding affinity tunes the dynamical behavior of system S . a-d all assume that $\rho_A = \rho_F = \rho$. Numerical simulations show the dynamical behavior of system S when changing ρ from 0 to 0.05 while other parameters are held to their nominal values of $\lambda_A = 0.08$, $\pi_A = 1.9$, $\lambda_F = 0.002$, $\pi_F = 0.058$, $\gamma_C = 0.025$, and $\delta_A = \delta_F = 0.0045$. From simulation results we can see that $\rho = 0.01$ gives sustained oscillations but other parameter choices give either steady states ($\rho = 0$ or 0.05) or damped oscillations ($\rho = 0.002$). We obtained similar simulation results by changing parameter γ_C .

To investigate the relationship between oscillations and the value of ρ and γ_C , we generated the root locus plots of the system (Figure 4.5). Analyzing a root locus is a graphical method to examine how variations of a parameter affect the roots (in this case the eigenvalues) of a system. In these two plots, there exists a range of ρ and γ_C for which the eigenvalues

have positive real part, corresponding to unstable fixed points indicating sustained oscillations. This informs us that tuning the DNA binding affinity and the auxin degradation strength in the ASRO could push the system into a sustained oscillatory regime. Mapping back to the circuit design of the ASRO, tuning the DNA binding affinity could be achieved through tuning the DNA binding domain of A or the corresponding binding sites in the promoter. This could be achieved experimentally by swapping out different DNA binding domains of A and corresponding promoters, or we can generate random mutations on the DNA binding domain or binding sites in the promoter. Tuning the auxin degradation strength could be achieved through swapping the IAA degron [26, 31] or varying the concentration of the auxin added to the ASRO.

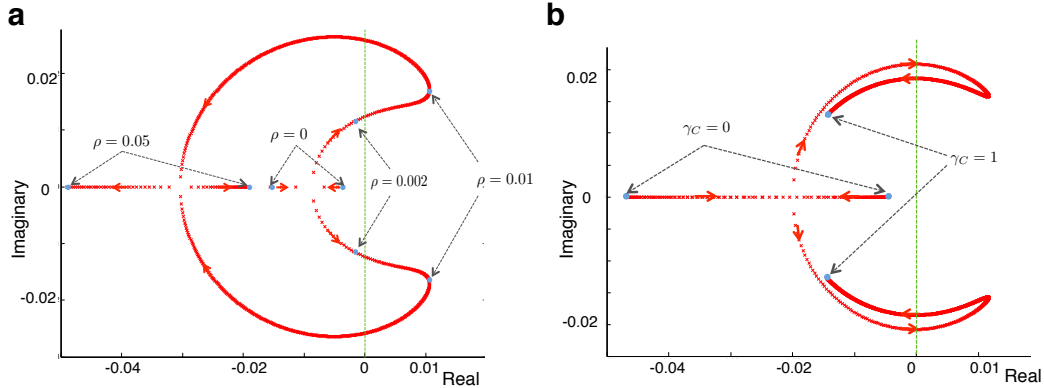


Figure 4.5: Root locus analysis of system S with respect to parameters $\rho_A = \rho_F = \rho$ and γ_C . (a) Numerical simulations show how the eigenvalues of system S change when changing parameter ρ from 0 to 0.5 with a step size of 0.0001. We marked out corresponding eigenvalues of system S when $\rho = 0, 0.002, 0.01$, and 0.05 . We see that the real parts of the eigenvalues when $\rho = 0.01$ are all positive, which satisfy conditions (i) and (ii), thus giving rise to sustained oscillations, while real parts of eigenvalues of $\rho = 0, 0.002, 0.05$ are all negative, thus generating stable solutions. These results can be cross-checked by numerical simulations in Figure 4.4. (b) Numerical simulations show how eigenvalues of system S change when changing parameter γ_C from 0 to 1 with a step size of 0.0001. We see that there is a range of γ_C where the real parts of eigenvalues are positive, which leads the system to display sustained oscillations. These two simulations inform us that tuning the DNA binding affinity and the auxin degradation strength in the ASRO could push the system into a sustained oscillatory regime.

4.5 High-throughput Testing Method: Time-seq

4.5.1 Motivation

We implemented the ASRO design with the ZAVNY shown in Chapter 2 as ASTA, and TIR1DM as FBox. Experimentally, this implementation did not generate sustained oscillations. The hypothesis is that the parameters did not fall into oscillatory regime. As shown from theoretical analysis in the previous section, one approach to obtain sustained oscillations is to tune the DNA binding affinity and the auxin degradation strength of the ASTA. Experimentally, the tuning approach could be building a library of ASTAs each with possibly different parameters and screen them to find the ones that oscillate. The probability of getting functional ASRO increases as library size increases, so we want a library size as large as possible. The traditional time course cytometry or microscopy approach for testing many dynamic gene circuits become unrealistic if the library size is on the order of thousands. Here, we propose Time-seq, a high-throughput testing method that uses next generation sequencing to gather time course data from thousands of dynamic gene circuit variants in a single tube.

4.5.2 Time-seq overview

Time-seq is a high-throughput testing method for gathering time course data of a library of dynamical circuits utilizing the power of next-generation RNA sequencing (RNA-Seq) [42]. This method was developed under the assumption that it is possible to associate the performance of each circuit in the library to specific RNA expression levels. For example, some dynamic gene circuits' behavior can be observed and quantified from the mRNA level of certain proteins, or through non-coding RNA level, such as circuits built with the CRISPR transcriptional control system [48] where small guide RNA level can be an indicator of the system functions. Under this assumption, we can track the performance of each circuit over time using RNA-seq. Under this assumption, we can track the performance of each circuit over time using RNA-seq. We concluded in the previous section that one approach to obtain

ASRO oscillations is to tune the DNA binding affinity and the auxin degradation strength, which can be achieved through mutagenizing domain I and domain II of the auxin-sensitive transcription activator (ASTA). Using error prone PCR, we can build a library of ASTAs, each with mutagenized domain I and domain II. This library is then transformed into target yeast strain to build a library of ASROs with variable DNA binding affinity and auxin degradation strength. In the previous sections, we showed that ASTA levels are a proxy for the oscillator performance. Moreover, ASTA mRNA unequivocally identifies the mutagenized gene in the library: this allows us to associate each circuit variant to its performance.

An overview of the Time-seq workflow is presented in Figure 4.6. After transforming mutagenized library into yeast strain, we then grow the library in a continuous device culture, for example, a large volume turbidostat, and harvest overtime and freeze them to preserve RNA state. Then we can extract RNA for all the samples, prepare the cDNAs for domains I and II part of the ASTA using primers with barcodes specific to the time point of each sample harvested at. Then we pool all the cDNAs samples as cDNA library to perform next generation sequencing using platform like Illumina MiSeq [3]. From the sequencing results, we will get sequences for each cDNA variant and the number of reads it appears in the samples. Using the time specific primer barcodes, we can recover which time point these cDNA sequences belong to. From the sequences of domain I and domain II, we can categorize which variant each cDNA sequence belongs to. Hence, we can recover the mRNA level of ASTA for each variant over time in the pooled sample.

The Time-seq method explained so far is prone to bias due to variations in sample harvesting, RNA extraction and cDNA preparation. Hence, we propose to pair cDNA preparation of ASTA mRNA, to cDNA preparation of a housekeeping gene, whose expression remains consistent across all cells states over time. By preparing the two cDNAs in the same batch, and using the same time specific primer barcodes, we can then rescale and normalize all the ASTA mRNA measurements.

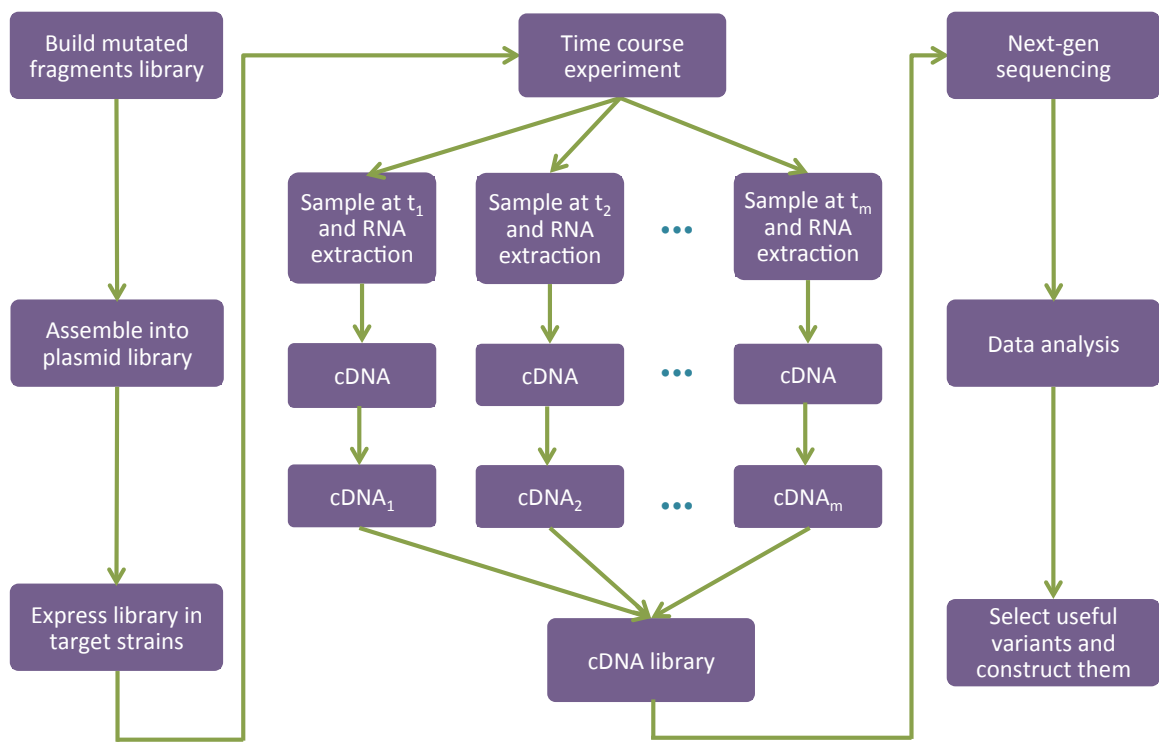


Figure 4.6: Overview of the Time-seq method workflow

4.6 Discussion

Time-seq is a novel method that utilizes the power of RNA-seq to get time course data for library of dynamical circuits. However, it remains to consider if Time-seq efficiency is affected by the library size, and if so how. In fact, a larger library size often provides better chance of getting the correct circuit and gives more data to learn how the system works. One needs to consider how library size affects the ability of Time-seq to faithfully track the dynamic of the circuit in each variant. With this aim in mind, we define a metric named data resolution R as the average number of reads per variant per time point. R could be calculated as $R = \frac{N}{MK}$ where N is the total number of reads from RNA-seq, M is number of time points tested, K is the library size of the dynamical circuits. The previous calculations for the ASRO reads uses this equation to estimate about 1000 reads per variant per time points given 1000 variants, 20 time points and 20 million total reads from Miseq 2x300 bp run. Notice that any other platform rather than Miseq 2x300 bp run could be used as long as it covers the 500 bp mRNA length template used in the ASRO library. The appropriate sequencing platform choice depends on the length of mRNA that needs to be sequenced. For example, if your desired sequence region is 300 bp, you may use Illumina NexSeq 500 platform [4] which could produce up to 400 million reads. Using the same data resolution and number of time points as before, reducing the sequence region to 300 bp increases the library size to 20000 circuits. Therefore, data resolution, read length, number of time points and platform selections are all fundamental variables that need to be considered when determining the library size to test.

4.7 Summary

In this chapter, we presented an auxin-sensitive relaxation oscillator (ASRO) design in yeast, performed a theoretical analysis to identify key parameters for its tuning, and proposed a high-throughput method called Time-seq for tuning ASRO. On the theoretical side, we first developed a detailed mathematical model involving genes, mRNAs, proteins and then

reduced it to a simple two-dimensional nonlinear dynamical model with general Hill function considerations. By using the Poincaré-Bendixson theorem, we deduced the requirements for the system to exhibit limit cycle oscillations. Building on these results, we studied how Hill coefficient affects sustained oscillations and proved that a Hill coefficient $n > 1$ is a necessary condition for our system to exhibit sustained oscillations. Through numerical simulations, we showed that tuning the DNA binding affinity and the auxin degradation strength in the ASRO could push the system into a sustained oscillatory regime. Finally, we addressed the problem of defining a high-throughput method for testing dynamic gene circuits such as oscillators. We proposed Time-seq, a high-throughput testing method that leverages next generation sequencing to gather time course data from thousands of oscillator variants in a single tube. We believe that high-throughput testing methods similar to what we proposed here will enable a faster and easier testing for dynamic gene circuits.

Chapter 5

BUILD AND TEST THE AQUARIUM WAY

For many synthetic biology projects, building and testing are the most repetitive, time consuming, and tedious components of the project. The build process largely involves molecular cloning, which is often labor intensive, prone to error, and low throughput when individual researchers carry out the cloning by themselves. The test process also requires expert knowledge of scientific instruments and experimental protocols. Many experimental processes in the build and test components are not well documented as they are carried out, which can give rise to reproducibility issues. [9]. There have been several industrial efforts to solve these problems using specialized robotics and software [11]. However, this remains a challenge in the academic setting, where specialized robots are expensive to afford and operate.

In this chapter, we present “Build and Test the Aquarium Way”, a software based human-in-the-loop automation solution to the build and test processes in synthetic biology without requiring specialized robotics. First, we introduce Aquarium, its inventory management scheme, and Krill protocol language. Second, we present the plasmid construction and yeast cloning processes, the build processes we developed in Aquarium. Third, we present the test processes we developed in Aquarium, the yeast cytometry process and the Cowfish package, which handles the automatic retrieval and labeling of cytometry data. With these build and test processes in Aquarium, researchers can view the build and test components of their projects as abstracted input-output functions and focus on high-level design and analysis.

5.1 Aquarium

Aquarium is a smart wetlab operating system developed in the Klavins Lab [1], which enables human-in-the-loop automation for synthetic biology lab work. In Aquarium, researchers enter inventory specifications and submit experiment orders, and lab technicians fulfill these orders following step-by-step instructions detailed in Aquarium. Aquarium is currently implemented as a web application using Ruby on Rails [5]. Aquarium compiles orders from individual researchers into step-by-step instructions presented to technicians in a web browser that can be displayed on a touch screen monitor or other computer devices. Aquarium builds an abstraction layer that separates the design and build components. Researchers can focus on design while the repetitive and labor intensive build process is carried out by lab technicians, guided by Aquarium-encoded instructions. Figure 5.4 illustrates the Aquarium process and the abstraction layer.

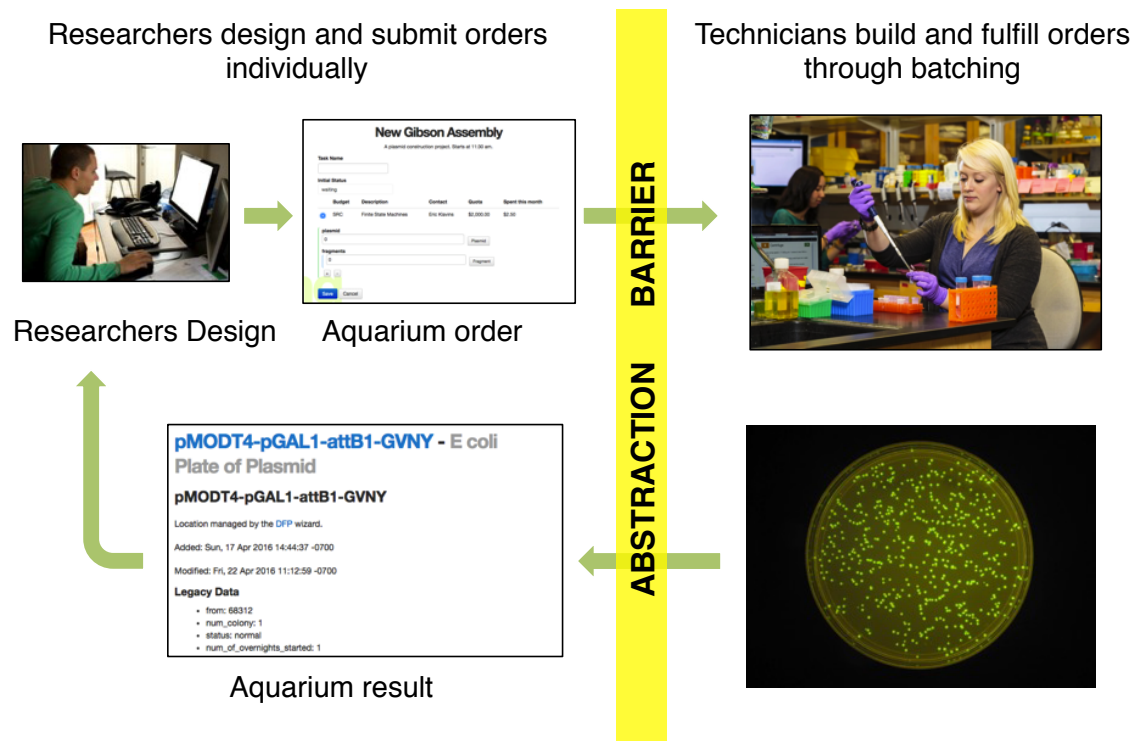


Figure 5.1: Aquarium overview: researchers design and technicians build

In order to formally specify what researchers are ordering and technicians are building in the lab, Aquarium consists of an underlying inventory management system where each physical item in the lab is modeled through the Aquarium inventory scheme shown in Figure 5.2. Each physical item is modeled as an *Item*. An *Item* has a *Container Type*, which models what kind of “container” this item is in. For example, a *Container Type* could be a *Plasmid Stock*, *Primer Aliquot*, *Yeast Plate*, *Glycerol Stock*, *Stripwell*, *96-Well Plate*, etc. An *Item* can be used to model an item such as 1.5 mL tube that contains one sample or a collection such as a 96-well plate containing multiple samples. Thus, an *Item* is modeled to have one or many *Samples*, where *Sample* models the sample inside the “container”. For example, both *Items* in Figure 5.2c and Figure 5.2d are of *Container Type Glycerol Stocks*. They each have one *Sample* in them, one is Plasmid pGALZ4-BleoMX, the other is Yeast Strain pGALZ4-BleoMX in W303a. In contrast, *Items* in Figure 5.2e and Figure 5.2f are a 8-well stripwell and a 96-well plate respectively. They both have many *Samples* in them: one contains 8 *Plasmids*, and the other contains 96 *Yeast Strains*. We also call these types of *Items* as *Collections*. We use 2D array to model the layout of the *Samples* in the *Item*. For example, 8 *Plasmids* are modeled by a 1x8 array and 96 *Yeast Strains* are modeled by an 8x12 array.

Samples are instances of *Samples Types*. *Sample Type* is an abstract class of the *Sample* to categorize different types of *Samples* in the lab. For example, a *Sample Type* could be a *Plasmid*, *Yeast Strain*, *Primer*, *Fragment*, etc. In Figure 5.2b, *Plasmid* pGALZ4-BleoMX is an instantiation of the *Sample Type Plasmid*. Under the *Sample Type Plasmid*, Length, Sequence, and Sequencing Primers are defined as properties. The instantiated *Plasmid* pGALZ4-BleoMX has defined Length, Sequence, and Sequencing Primers filled in. Other than *Container Type* and *Sample*, each *Item* also has *Data* and a *Location* associated with it. *Data* accepts any valid JSON (JavaScript Object Notation) string. *Location* is a string that uniquely identifies where the *Item* is located in the lab.

Mapping to the implementation of Aquarium as a Rails application, *Item*, *Container type*, *Sample*, and *Sample Type* each corresponds to an Active Record model/class tying to

a database table. Therefore each *Item*, *Container type*, *Sample*, and *Sample Type* have a unique database id in the corresponding database table. For example, *Item* 12452 in Figure 5.2a has a unique id of 12452 in the database table.

In order to specify how to manipulate items stored in the inventory and show step-by-step instructions to technicians, Domain-specific languages (DSL) were developed in Aquarium for encoding protocols [1]. The DSL for encoding protocol is called Krill, which is based on a popular programming language Ruby [38]. The Krill protocol can be executed and displayed as step-by-step instructions for technicians to follow and interact with. Aquarium displays the protocol as interactive webpages using a combination of text descriptions, input forms, check boxes, dropdown select lists, tables, pictures, etc. Technicians follow these instructions to generate, use, update, and destroy items by performing actual lab work. Figure 5.3 illustrates the Krill code and the step-by-step instructions Aquarium produces.

5.2 Build the Aquarium Way: Plasmid Construction and Yeast Cloning

5.2.1 Plasmid Construction Process

We developed a plasmid construction process in Aquarium to enable researchers to construct novel plasmids from fragments using the Gibson assembly method [21]. Figure 5.4 illustrates the plasmid construction process. The process consists of five workflows: Primer Order, Fragment Construction, Gibson Assembly, Plasmid Verification, and Glycerol Stock. Each workflow takes a set of inputs, and consists of a series of protocols to execute sequentially to produce the specified outputs. For example, Primer Order workflow takes *Primer* as input and produces *Primer Stocks* and *Primer Aliquots* as outputs through the execution of *order_primer* protocol and *stock_primer* protocol.

A typical plasmid construction process only requires researchers to submit Gibson Assembly orders. A Gibson Assembly order requires inputs of *Plasmids* and *Fragments* whereas outputs are *E.coli Plate of Plasmid* items. Once a Gibson Assembly order is received, the process checks the inputs of the order with specified input requirements. If the requirements

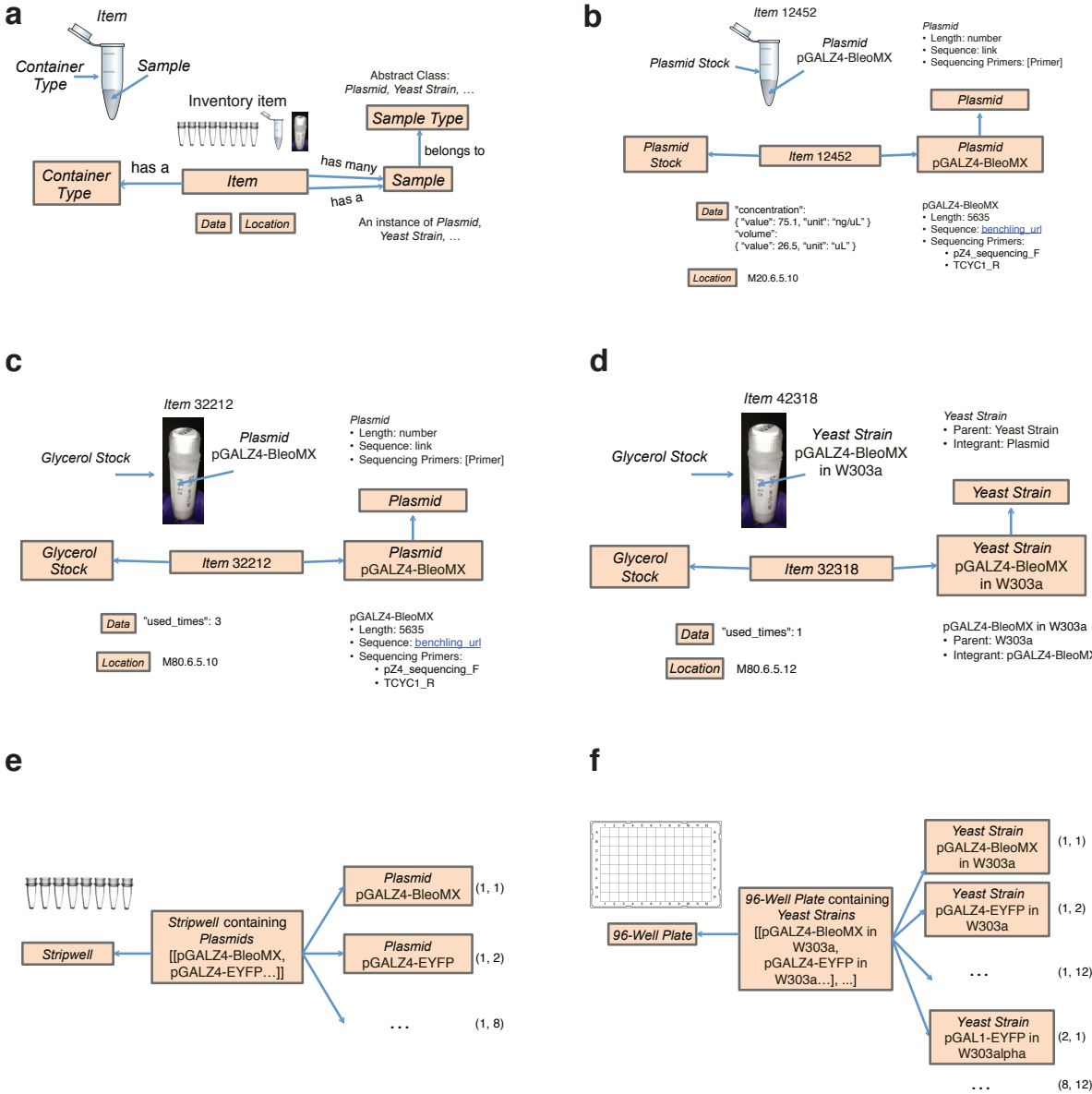


Figure 5.2: Aquarium inventory scheme. (a) The inventory scheme overview. (b) An *Item* with *Container Type* of *Plasmid Stock* and *Sample* of *Plasmid pGALZ4-BleoMX*. (c) An *Item* with *Container Type* of *Glycerol Stock* and *Sample* of *Plasmid pGALZ4-BleoMX*. (d) An *Item* with *Container Type* of *Glycerol Stock* and *Sample* of *Yeast Strain pGALZ4-BleoMX in W303a*. (e) An *Item* with *Container Type* of *Stripwell* and has a 1x8 *Sample* array. (f) An *Item* with *Container Type* of *96-Well Plate* and has an 8x12 *Sample* array.

a

<p>Instructions</p> <p>Krill code</p>	<div style="border: 1px solid #ccc; padding: 10px; background-color: #f9f9f9;"> <p>Job 28500 / Metacol 5920 squilib/workflows/ecoli/gibson.rb</p> <p>History Associations Actions</p> <p>6:53:30 PM Gibson Assembly Information</p> <p>1 Gibson Assembly Information OK</p> <p>In this protocol, you will build 2 plasmids using Gibson Assembly method.</p> <p>The predicted time needed is 29 min.</p> <p>vang</p> <pre>predicted_time = time_prediction fragment_stocks_flatten.length, "gibson" # Tell the user what we are doing show { title "Gibson Assembly Information" note "In this protocol, you will build #{io_hash[:plasmid_ids].length} plasmids using Gibson Assembly method." note "The predicted time needed is #{predicted_time} min."</pre> </div>
---------------------------------------	---

b

<p>Instructions</p> <p>Krill code</p>	<div style="border: 1px solid #ccc; padding: 10px; background-color: #f9f9f9;"> <p>Job 28500 / Metacol 5920 squilib/workflows/ecoli/gibson.rb</p> <p>History Associations Actions</p> <p>6:53:30 PM Gibson Assembly Information</p> <p>7:02:10 PM Boxes Required</p> <p>7:02:13 PM Take from M20.0.4</p> <p>7:02:56 PM Take from M20.5.1</p> <p>4 Take from M20.5.1 OK</p> <p>Collect Item(s)</p> <table border="1" style="width: 100%; border-collapse: collapse;"> <thead> <tr> <th>0</th><th>1</th><th>2</th><th>3</th><th>4</th><th>5</th><th>6</th><th>7</th><th>8</th></tr> </thead> <tbody> <tr><td>9</td><td>10</td><td>11</td><td>12</td><td>13</td><td>14</td><td>15</td><td>16</td><td>17</td></tr> <tr><td>18</td><td>19</td><td>20</td><td>21</td><td>22</td><td>23</td><td>24</td><td>25</td><td>26</td></tr> <tr><td>27</td><td>28</td><td>29</td><td>30</td><td>31</td><td>32</td><td>33</td><td>34</td><td>35</td></tr> <tr><td>36</td><td>37</td><td>38</td><td>39</td><td>40</td><td>41</td><td>42</td><td>43</td><td>44</td></tr> <tr><td>45</td><td>46</td><td>47</td><td>48</td><td>49</td><td>50</td><td>51</td><td>52</td><td>53</td></tr> <tr><td>54</td><td>55</td><td>56</td><td>57</td><td>58</td><td>59</td><td>60</td><td>61</td><td>62</td></tr> <tr><td>63</td><td>64</td><td>65</td><td>66</td><td>67</td><td>68</td><td>69</td><td>70</td><td>71</td></tr> <tr><td>72</td><td>73</td><td>74</td><td>75</td><td>76</td><td>77</td><td>78</td><td>79</td><td>80</td></tr> </tbody> </table> <p>vand</p> <pre># Take fragment stocks take fragment_stocks_flatten, interactive: true, method: "boxes" # Prompt users to measure concentration if concentration data does not exist ensure_stock_concentration fragment_stocks_flatten # Verify volumes of the fragment stock verify_stock_volumes fragment_stocks_flatten</pre> </div>	0	1	2	3	4	5	6	7	8	9	10	11	12	13	14	15	16	17	18	19	20	21	22	23	24	25	26	27	28	29	30	31	32	33	34	35	36	37	38	39	40	41	42	43	44	45	46	47	48	49	50	51	52	53	54	55	56	57	58	59	60	61	62	63	64	65	66	67	68	69	70	71	72	73	74	75	76	77	78	79	80
0	1	2	3	4	5	6	7	8																																																																										
9	10	11	12	13	14	15	16	17																																																																										
18	19	20	21	22	23	24	25	26																																																																										
27	28	29	30	31	32	33	34	35																																																																										
36	37	38	39	40	41	42	43	44																																																																										
45	46	47	48	49	50	51	52	53																																																																										
54	55	56	57	58	59	60	61	62																																																																										
63	64	65	66	67	68	69	70	71																																																																										
72	73	74	75	76	77	78	79	80																																																																										

Figure 5.3: Aquarium Krill Protocol Examples. (a) Text instructions shown to the technician on a webpage. (b) Box layout illustration to guide technician to retrieve an inventory item from a 9x9 freezer box.

are fulfilled, the order will be pushed to a ready queue to be executed in batch with other ready Gibson Assembly orders, and technicians are instructed to run the protocols in the Gibson Assembly workflow. If the requirements are not fulfilled, it will trigger other workflow orders to fulfill the requirements or inform researchers that information input is required. For example, the Gibson Assembly order inputs require the *Fragment* to have a corresponding *Fragment Stock* in the inventory for the Gibson Assembly order to move to the ready queue. If a Gibson Assembly order's inputs specify a *Fragment* that does not have a *Fragment Stock* ready, the process will intelligently submit a Fragment Construction order with inputs and outputs entered automatically to produce that required *Fragment Stock*. Same backtracking processes happens here when a Fragment Construction order is submitted. It will trigger an automatic submission of a Primer Order workflow order if a *Primer Aliquot* is needed for the Fragment Construction order.

This process of backtracking inputs enables the researchers to only enter a Gibson Assembly order once and have all required orders automatically triggered by the process. Meanwhile, the individual workflow architecture gives flexibility to researcher to use any workflow on demand. For example, a researcher who only need to construct a few fragments can enter individual Fragment Construction orders without using other workflows in the plasmid construction process.

After the execution of each workflow, as shown in Figure 5.4, there is an output decision point. Unsuccessful execution of the workflow order may trigger a re-run of the order under the discretion of the researcher. For example, if a Fragment Construction failed to produce the desired Fragment Stock, it triggers a suggested re-run of the order but requires the approval of the researcher. For some workflows, successful execution may trigger other workflow orders. For example, a successful Gibson Assembly order execution will automatically trigger a Plasmid Verification order. The automatic generated inputs are *E.coli Plate of Plasmid* from the Gibson Assembly order outputs, a default of one colony to screen, and associated sequencing primers that are defined in the corresponding *Plasmid*. The outputs are a *Plasmid Stocks*, *TB overnight of Plasmids*, and sequencing results files. The Plas-

mid Verification workflow executes overnight, miniprep, sequencing, and upload sequencing results protocols to produce these outputs. After a successful Plasmid Verification order, a Glycerol Stock order will be automatically triggered to produce a *Glycerol Stock* for the sequence verified plasmid after the researcher verifies the sequencing results for each *Plasmid Stock* item.

With the input backtracking and output decision, researchers can complete the entire plasmid construction process by entering only a Gibson Assembly order and indicating which *Plasmid Stock* to create a *Glycerol Stock* for after receiving sequencing results from Aquarium. By November 2016, the plasmid construction process in Aquarium enabled researchers at the University of Washington to build over 8,000 novel plasmids without the researchers ever performing the cloning protocols themselves. This enabled the researchers to view the plasmid construction as an abstract process so they can focus on the high level experimental design of their synthetic biology projects.

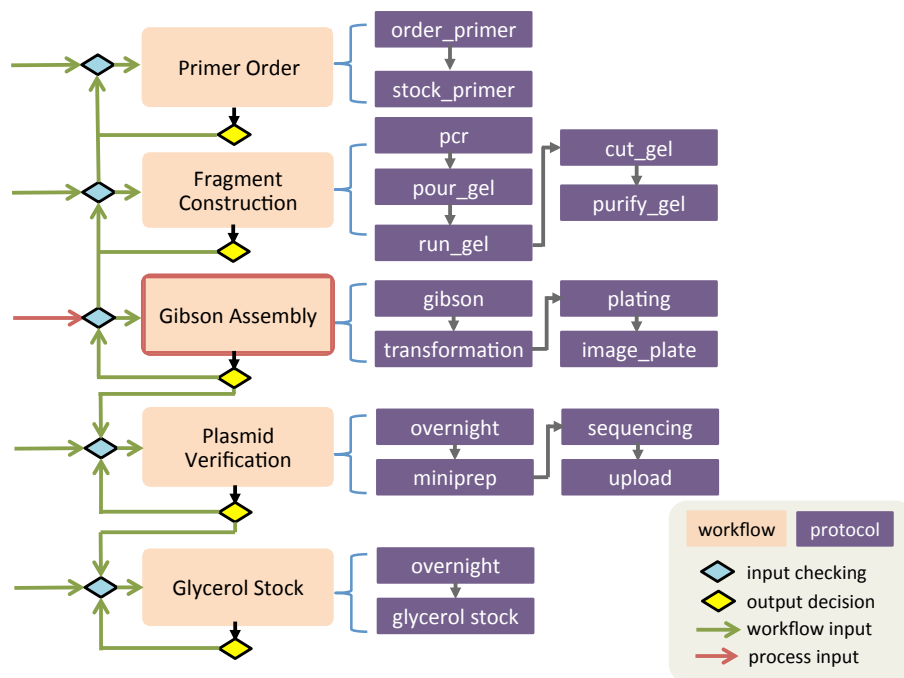


Figure 5.4: Overview of plasmid construction process in Aquarium

5.2.2 Yeast Cloning Process

We developed a yeast cloning process in Aquarium to enable researchers to construct novel yeast strains using standard lithium acetate yeast transformation protocol [22]. Figure 5.5 illustrates the yeast cloning process. The process consists of five workflows: Streak Plate, Yeast Competent Cell, Yeast Transformation, Yeast Strain QC, and Glycerol Stock.

A typical yeast cloning process only requires researchers to submit Yeast Transformation orders. A Yeast Transformation order requires inputs of a *Yeast Strain* and *Yeast Competent Cells*, and the outputs produce *Yeast Plates*. Once a Yeast Transformation order is received, the process checks whether *Yeast Competent Cells* are available in the inventory. If available, it will push the order to the ready queue, whereas if not available, it will keep the order in the waiting queue and automatically trigger a Yeast Competent Cell order to produce *Yeast Competent Cells*. The Yeast Competent Cell order requires inputs of *Divided Yeast Plates*. If the *Divided Yeast Plates* are not available in the inventory, it will trigger a Streak Plate order to produce *Divided Yeast Plates*. Thus, these backtracking procedures work similarly to those described in the plasmid construction process.

Once a Yeast Transformation order is completed, if it successfully produces a *Yeast Plate* with a positive number of colonies, it will trigger a Yeast Strain QC order. Yeast QC order executes through lysate, PCR, and gel protocols to produce a Gel Lane to verify whether the expected length of gel show up or not. If a gel band of the correct length is present, a Glycerol Stock order is triggered to start an overnight from that colony to make a *Glycerol Stock*. Noting that the Glycerol Stock workflow here is actually the same as the Glycerol Stock workflow detailed in the plasmid construction process. We designed these workflows to be modular so that they could accommodate requirements of various processes.

Using the yeast cloning process, researchers can build novel yeast strains by only entering a Yeast Transformation order in Aquarium, which results in *Glycerol Stocks* made from QC verified colonies. By November 2016, the yeast cloning process in Aquarium enabled researchers at the University of Washington to build over 7,000 novel yeast strains without

the researchers ever performing the cloning protocols themselves. This enabled researchers to view the yeast cloning as an abstract process so they can focus on the high level experimental design of their projects.

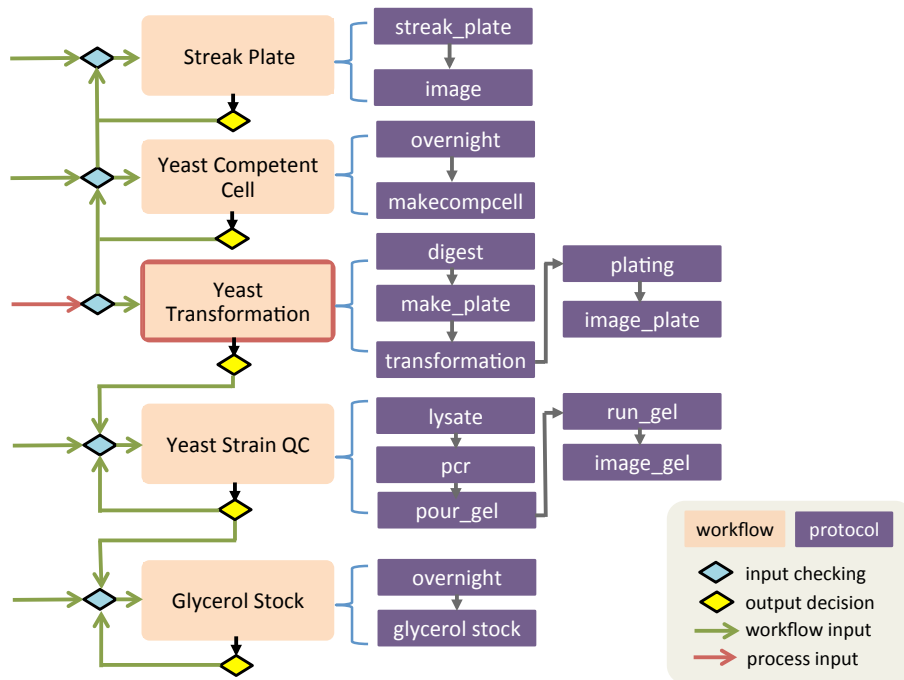


Figure 5.5: Overview of yeast cloning process in Aquarium

5.3 Test the Aquarium Way: Yeast Cytometry and Cowfish

5.3.1 Yeast Cytometry Process

Flow cytometry is one of the most common assays in synthetic biology for testing yeast strains. We developed a yeast cytometry process in Aquarium to perform time course cytometry assay on yeast strains. Figure 5.6.a illustrates the yeast cytometry process. The process consists of only two workflows: Streak Plate and Yeast Cytometry. The process starts with a Yeast Cytometry order, which requires *Divided Yeast Plates* as an input. It backtracks to trigger a Streak Plate order if no *Divided Yeast Plate* is in the inventory. Once

the Yeast Cytometry order is ready after the input requirements are fulfilled, it begins with a yeast overnight from the *Divided Yeast Plate*. A dilution is then performed, followed by cytometry read(s) with a customizable number of reads, dilutions, and time intervals between reads and dilutions. Note that there are arrows going back from read to both read and dilution, which indicates that researchers can specify the timeline of dilutions and reads as they desire. Figure 5.6.b gives an example of a dilution and read timeline, where researchers specify a read every 8 h and a dilution every 16 h. In this case, both a dilution and a read occurs at 0, 16, and 32h, and researchers can specify whether dilution or read happens first. In this example, dilution happens before read, so dilution is placed above read in the illustration. Researchers also have the flexibility to specify the dilution rate and what type of media and inducers to use at each dilution. This Yeast Cytometry process in Aquarium is flexible enough to handle researcher's various requirements in using flow cytometry to test yeast strains.

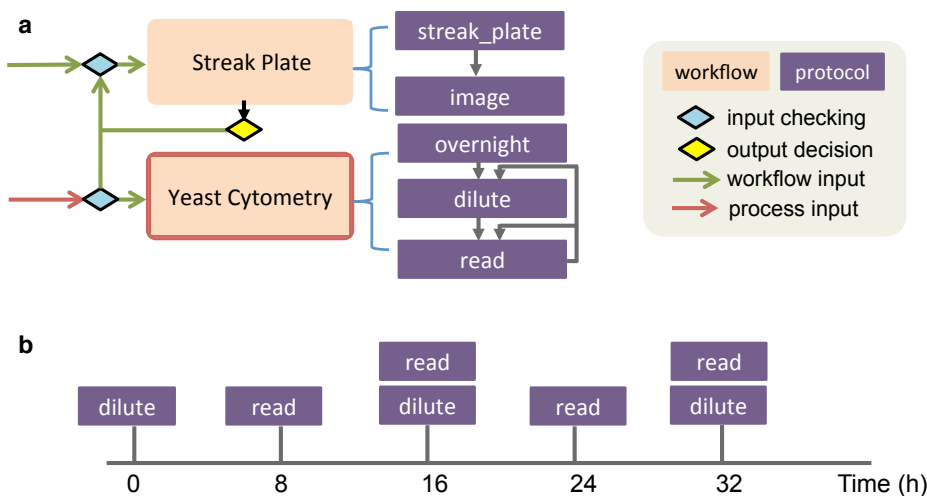


Figure 5.6: Yeast cytometry process in Aquarium (a) Flow chart overview of the yeast cytometry process (b) Example of a possible dilution read schedule.

5.3.2 Cowfish Package for Yeast Cytometry Data Retrieval and Labeling

After each read in the yeast cytometry process, the cytometry results are uploaded into Aquarium and associated with each digital log of the protocol job. Aquarium has an API for programmable access to its inventory data and job logs. We developed a Python package named Cowfish that utilizes the Aquarium API to retrieve the uploaded cytometry data and perform automatic data labeling. The package is open source. Source code and instructions for use of the package is on Github (<https://github.com/klavinslab/cowfish>). To use the Cowfish package, researchers must specify which cytometry read to analyze by providing the job id of the cytometry read. Cowfish will download the cytometry results data as a zipped collection of FCS files from Aquarium. It unzips the data, utilizes FlowCytometryTools package [2] and customized gate settings to parse the FCS files into Pandas dataframe, and labels each row of the dataframe with the sample name and inducer condition retrieved from the Aquarium job log of the cytometry read. In the end, it produces a dataframe similar to the one shown in Figure 5.7. The researchers are now in a good position to perform their desired data analysis and visualization on the dataframe that contains the summary of their cytometry results with automatic labeled information. The time course cytometry experimental results shown in Figure 2.2 was performed using this yeast cytometry process in Aquarium and the data was prepared using the Cowfish package.

Pandas DataFrame Index	conc	events	FL1A_mean	FL1A_sd	vol	sample_name	inducer_condition
7/5/16 10:05	283.365	1051	527.992388	525	3.709	TIR1_DM, pGALZ4-Z4AVNY, pACT1-ZEV4	None
7/5/16 10:06	225.01	1130	535.038938	496	5.022	TIR1_DM, pGALZ4-Z4AVNY, pACT1-ZEV4	100 nM b-e
7/5/16 10:06	93.3417	1336	579.830838	562	14.313	TIR1_DM, pGALZ4-Z4AVNY, pACT1-ZEV4	20 μ M auxin

Figure 5.7: Cowfish Dataframe Example. The dataframe is indexed by the absolute time that sample was passed through the cytometer. *conc* stands for the concentration of the processed yeast sample, *events* stands for number of events detected, *FL1A_mean* is the mean of the fluorescence data reported by the cytometer, *FL1A_sd* is the standard deviation, *vol* is the volume of the samples passed in the cytometer, *sample_name* and *inducer_condition* are information retrieved from the Aquarium job log and automatically aligned with the cytometry data.

5.4 Summary

In this chapter, we presented an overview of the Aquarium software, specifically the abstraction barrier between researchers and technicians, the inventory scheme, and the Krill protocol for formally defining the procedures in the lab as executable computer code. Built upon Aquarium, we developed the build processes: the plasmid construction process for building novel plasmids and the yeast cloning process for building novel yeast strains. The plasmid construction and yeast cloning processes enabled researchers to execute the build process as an abstracted input-output function. To abstract the test process, we developed the yeast cytometry process in Aquarium for testing yeast strains using flow cytometry, which enabled researchers to execute and plan flexible time course cytometry. The Cowfish package we developed enables automatic data retrieval and labeling for the yeast cytometry process. Yeast cytometry process and the Cowfish package enables researchers to submit yeast cytometry orders to Aquarium and receive labeled, pre-processed data available to perform downstream analysis and visualization. Obviously, there are more build and test processes that people are using in synthetic biology. We built these specific processes in Aquarium as they were most commonly used in the Klavins lab and contain the requirements and complexity to be handled by the software-enabled human-in-the-loop automation platform. These build and test processes serve as examples for researchers interested in building more Aquarium processes to automate other build and test processes in synthetic biology and beyond.

Chapter 6

CONCLUSIONS

Dynamic gene circuits are at the core of biological systems. Designing, building, and testing synthetic dynamic gene circuits such as bistable switches and oscillators are major pursuits in synthetic biology since the establishment of the field. In this thesis, we presented works on the design, construction, and validation of dynamic gene circuits in the yeast *Saccharomyces cerevisiae*, a model eukaryote, where there has been significantly less synthetic biology research and dynamic gene circuits are generally considered much more difficult to construct in yeast than in *E.coli*. In Chapter 2, we presented works on the design, build, and test components on a working bistable switch in yeast as one of the major milestones in building synthetic dynamic gene circuits in yeast. Experimental time course cytometry results were presented to show the bistability and switchability of the switch. Mathematical models were developed to both fit the experimental data and explain the bistability of the bistable switch. In Chapter 3, we presented works on an antibiotic resistance memory built with the bistable switch as one of the applications of the bistable switch. Experimental plate reader yeast growth data was presented to show the bistability of the growth rate for the resistance memory. Mathematical models were developed as an extension to the bistable switch to fit the growth data. In Chapter 4, we presented the design and analysis of an auxin sensitive relaxation oscillator (ASRO) in yeast and proposed possible directions to tune the oscillator. In Chapter 5, we presented “Build and Test the Aquarium Way”, and demonstrated how we improved the build and test processes with a software based human-in-the-loop automation platform to make engineering synthetic dynamic gene circuits easier in yeast.

There is still much work to be done to make designing, building, and testing dynamic

gene circuits in yeast easier, faster, and higher throughput. More types and variants of dynamic gene circuits such as multi-state memory, oscillators, dynamic logic, etc should be built and tested to truly understand the mechanisms in making dynamical behavior in yeast and similar eukaryotic cells. High throughput approaches similar to what we proposed in Chapter 4 could be developed by leveraging next generation sequencing or other high throughput test methods to truly increase the magnitude of circuits tested in each batch. Designing, building, and testing synthetic dynamic circuits could lead the way to harnessing the power of dynamics in cells.

BIBLIOGRAPHY

- [1] Aquarium. <http://klavinslab.org/aquarium.html>. Accessed: 2016-11-21.
- [2] Flowcytometrytools. <http://eyurtsev.github.io/FlowCytometryTools/>. Accessed: 2016-11-21.
- [3] Illumina miseq sequencer. <http://www.illumina.com/systems/miseq.html>. Accessed: 2015-4-29.
- [4] Illumina nextseq 500 desktop sequencer. <http://www.illumina.com/systems/nextseq-sequencer.html>. Accessed: 2015-4-29.
- [5] Ruby on rails. <http://rubyonrails.org/>. Accessed: 2016-11-21.
- [6] Caroline M Ajo-Franklin, David A Drubin, Julian A Eskin, Elaine PS Gee, Dirk Landgraf, Ira Phillips, and Pamela A Silver. Rational design of memory in eukaryotic cells. *Genes & development*, 21(18):2271–2276, 2007.
- [7] M. R. Atkinson, M. A. Savageau, J. T. Myers, and A. J. Ninfa. Development of genetic circuitry exhibiting toggle switch or oscillatory behavior in Escherichia coli. *Cell*, 113(5):597–607, May 2003.
- [8] Attila Becskei, Bertrand Séraphin, and Luis Serrano. Positive feedback in eukaryotic gene networks: cell differentiation by graded to binary response conversion. *The EMBO journal*, 20(10):2528–2535, 2001.
- [9] C Glenn Begley and Lee M Ellis. Drug development: Raise standards for preclinical cancer research. *Nature*, 483(7391):531–533, 2012.
- [10] Benjamin A Blount, Tim Weenink, and Tom Ellis. Construction of synthetic regulatory networks in yeast. *FEBS letters*, 586(15):2112–2121, 2012.
- [11] Hayden E Check. The automated lab. *Nature*, 516(7529):131–132, 2014.
- [12] Charles P Collier, Gunter Mattersteig, Eric W Wong, Yi Luo, Kristen Beverly, José Sampaio, Francisco M Raymo, J Fraser Stoddart, and James R Heath. A [2] catenane-based solid state electronically reconfigurable switch. *Science*, 289(5482):1172–1175, 2000.

- [13] Tal Danino, Octavio Mondragón-Palomino, Lev Tsimring, and Jeff Hasty. A synchronized quorum of genetic clocks. *Nature*, 463(7279):326–330, 2010.
- [14] D Del Vecchio. Design and analysis of an activator-repressor clock in e. coli. In *American Control Conference, 2007. ACC'07*, pages 1589–1594. IEEE, 2007.
- [15] Tom Ellis, Xiao Wang, and James J Collins. Diversity-based, model-guided construction of synthetic gene networks with predicted functions. *Nature biotechnology*, 27(5):465–471, 2009.
- [16] M. B. Elowitz and S. Leibler. A synthetic oscillatory network of transcriptional regulators. *Nature*, 403(6767):335–338, Jan 2000.
- [17] LilyAnn Novak Frazer and Raymond T O’Keefe. A new series of yeast shuttle vectors for the recovery and identification of multiple plasmids from *saccharomyces cerevisiae*. *Yeast*, 24(9):777–789, 2007.
- [18] Ari E Friedland, Timothy K Lu, Xiao Wang, David Shi, George Church, and James J Collins. Synthetic gene networks that count. *Science*, 324(5931):1199–1202, 2009.
- [19] E. Fung, W. W. Wong, J. K. Suen, T. Bulter, S. G. Lee, and J. C. Liao. A synthetic gene-metabolic oscillator. *Nature*, 435(7038):118–122, May 2005.
- [20] T. S. Gardner, C. R. Cantor, and J. J. Collins. Construction of a genetic toggle switch in *escherichia coli*. *Nature*, 403(6767):339–342, 2000.
- [21] D. G. Gibson, L. Young, R. Chuang, J. C. Venter, C. A Hutchison, and H. O. Smith. Enzymatic assembly of dna molecules up to several hundred kilobases. *Nature methods*, 6(5):343–345, 2009.
- [22] R Daniel Gietz and Robin A Woods. Transformation of yeast by lithium acetate/single-stranded carrier dna/polyethylene glycol method. *Methods in enzymology*, 350:87–96, 2002.
- [23] E. Giniger and M. Ptashne. Cooperative dna binding of the yeast transcriptional activator gal4. *Proceedings of the National Academy of Sciences*, 85(2):382–386, 1988.
- [24] R. Guantes and J. F. Poyatos. Dynamical principles of two-component genetic oscillators. *PLoS Comput. Biol.*, 2(3):e30, Mar 2006.
- [25] Robin E Harris, Michael Pargett, Catherine Sutcliffe, David Umulis, and Hilary L Ashe. Brat promotes stem cell differentiation via control of a bistable switch that restricts bmp signaling. *Developmental cell*, 20(1):72–83, 2011.

- [26] Kyle A Havens, Jessica M Guseman, Seunghee S Jang, Edith Pierre-Jerome, Nick Bolten, Eric Klavins, and Jennifer L Nemhauser. A synthetic approach reveals extensive tunability of auxin signaling. *Plant physiology*, 160(1):135–142, 2012.
- [27] J. Higgins. A chemical mechanism for oscillation of glycolytic intermediates in yeast cells. *Proceedings of the National Academy of Sciences of the United States of America*, 51(6):989, 1964.
- [28] Brian D Jensen, Matthew B Parkinson, Katsuo Kurabayashi, Larry L Howell, and Michael S Baker. Design optimization of a fully-compliant bistable micro-mechanism. *Ann Arbor MI*, 48109:2125, 2001.
- [29] Andrew D Keller. Specifying epigenetic states with autoregulatory transcription factors. *Journal of theoretical biology*, 170(2):175–181, 1994.
- [30] Andrew D Keller. Model genetic circuits encoding autoregulatory transcription factors. *Journal of Theoretical Biology*, 172(2):169–185, 1995.
- [31] Arjun Khakhar, Nicholas J Bolten, Jennifer Nemhauser, and Eric Klavins. Cell–cell communication in yeast using auxin biosynthesis and auxin responsive crispr transcription factors. *ACS synthetic biology*, 5(4):279–286, 2015.
- [32] Ahmad S Khalil and James J Collins. Synthetic biology: applications come of age. *Nature Reviews Genetics*, 11(5):367–379, 2010.
- [33] T. Kondo. A cyanobacterial circadian clock based on the Kai oscillator. *Cold Spring Harb. Symp. Quant. Biol.*, 72:47–55, 2007.
- [34] B. P. Kramer, A. U. Viretta, D. M. Baba, D. Aubel, W. Weber, and M. Fussenegger. An engineered epigenetic transgene switch in mammalian cells. *Nature biotechnology*, 22(7):867–870, 2004.
- [35] Karen Lai, Matthew J Robertson, and David V Schaffer. The sonic hedgehog signaling system as a bistable genetic switch. *Biophysical journal*, 86(5):2748–2757, 2004.
- [36] T. Lebar, U. Bezeljak, A. Golob, M. Jerala, L. Kadunc, B. Pirš, M. Stražar, D. Vučko, U. Zupančič, M. Benčina, et al. A bistable genetic switch based on designable dna-binding domains. *Nature communications*, 5, 2014.
- [37] Mats Lundgren, Lena Ström, Lars-Olof Bergquist, Sven Skog, Thomas Heiden, Janet Stavnezer, and Eva Severinson. Cell cycle regulation of immunoglobulin class switch recombination and germ-line transcription: potential role of ets family members. *European journal of immunology*, 25(7):2042–2051, 1995.

- [38] Yukio Matsumoto and K Ishituka. Ruby programming language, 2002.
- [39] R. S. McIsaac, S. J. Silverman, M. N. McClean, P. A. Gibney, J. Macinskas, M. J. Hickman, A. A. Petti, and D. Botstein. Fast-acting and nearly gratuitous induction of gene expression and protein depletion in *saccharomyces cerevisiae*. *Molecular biology of the cell*, 22(22):4447–4459, 2011.
- [40] R Scott McIsaac, Benjamin L Oakes, Xin Wang, Krysta A Dummit, David Botstein, and Marcus B Noyes. Synthetic gene expression perturbation systems with rapid, tunable, single-gene specificity in yeast. *Nucleic acids research*, page gks1313, 2012.
- [41] Tae Seok Moon, Chunbo Lou, Alvin Tamsir, Brynne C Stanton, and Christopher A Voigt. Genetic programs constructed from layered logic gates in single cells. *Nature*, 491(7423):249–253, 2012.
- [42] Fatih Ozsolak and Patrice M Milos. Rna sequencing: advances, challenges and opportunities. *Nature reviews genetics*, 12(2):87–98, 2011.
- [43] E. Pierre-Jerome, S. S. Jang, K. A. Havens, J. L. Nemhauser, and E. Klavins. Recapitulation of the forward nuclear auxin response pathway in yeast. *Proceedings of the National Academy of Sciences*, 111(26):9407–9412, 2014.
- [44] C. S. Pittendrigh. Circadian rhythms and the circadian organization of living systems. In *Cold Spring Harbor symposia on quantitative biology*, volume 25, pages 159–184. Cold Spring Harbor Laboratory Press, 1960.
- [45] Joseph R Pomerening, Sun Young Kim, and James E Ferrell. Systems-level dissection of the cell-cycle oscillator: bypassing positive feedback produces damped oscillations. *Cell*, 122(4):565–578, 2005.
- [46] Priscilla EM Purnick and Ron Weiss. The second wave of synthetic biology: from modules to systems. *Nature reviews Molecular cell biology*, 10(6):410–422, 2009.
- [47] Priscilla EM Purnick and Ron Weiss. The second wave of synthetic biology: from modules to systems. *Nature reviews Molecular cell biology*, 10(6):410–422, 2009.
- [48] Lei S Qi, Matthew H Larson, Luke A Gilbert, Jennifer A Doudna, Jonathan S Weissman, Adam P Arkin, and Wendell A Lim. Repurposing crispr as an rna-guided platform for sequence-specific control of gene expression. *Cell*, 152(5):1173–1183, 2013.

- [49] Dae-Kyun Ro, Eric M Paradise, Mario Ouellet, Karl J Fisher, Karyn L Newman, John M Ndungu, Kimberly A Ho, Rachel A Eachus, Timothy S Ham, James Kirby, et al. Production of the antimalarial drug precursor artemisinic acid in engineered yeast. *Nature*, 440(7086):940–943, 2006.
- [50] N. Rosenfeld, J. W. Young, U. Alon, P. S. Swain, and M. B. Elowitz. Gene regulation at the single-cell level. *Science*, 307(5717):1962–1965, 2005.
- [51] Wiep Klaas Smits, Oscar P Kuipers, and Jan-Willem Veening. Phenotypic variation in bacteria: the role of feedback regulation. *Nature Reviews Microbiology*, 4(4):259–271, 2006.
- [52] Dennis W Stacey. Cyclin d1 serves as a cell cycle regulatory switch in actively proliferating cells. *Current opinion in cell biology*, 15(2):158–163, 2003.
- [53] J. Stricker, S. Cookson, M. R. Bennett, W. H. Mather, L. S. Tsimring, and J. Hasty. A fast, robust and tunable synthetic gene oscillator. *Nature*, 456(7221):516–519, Nov 2008.
- [54] Chris N Takahashi, Aaron W Miller, Felix Ekniss, Maitreya J Dunham, and Eric Klavins. A low cost, customizable turbidostat for use in synthetic circuit characterization. *ACS synthetic biology*, 4(1):32–38, 2014.
- [55] M. Tigges, T. T. Marquez-Lago, J. Stelling, and M. Fussenegger. A tunable synthetic mammalian oscillator. *Nature*, 457(7227):309–312, Jan 2009.
- [56] G. TJ. Van Der Horst, M. Muijtjens, K. Kobayashi, R. Takano, S. Kanno, M. Takao, J. de Wit, A. Verkerk, A. PM. Eker, D. van Leenen, et al. Mammalian cry1 and cry2 are essential for maintenance of circadian rhythms. *Nature*, 398(6728):627–630, 1999.
- [57] J. MG. Vilar, H. Y. Kueh, N. Barkai, and S. Leibler. Mechanisms of noise-resistance in genetic oscillators. *Proceedings of the National Academy of Sciences*, 99(9):5988–5992, 2002.
- [58] Baojun Wang, Richard I Kitney, Nicolas Joly, and Martin Buck. Engineering modular and orthogonal genetic logic gates for robust digital-like synthetic biology. *Nature communications*, 2:508, 2011.
- [59] Lei Wang, Brandon L Walker, Stephen Iannaccone, Devang Bhatt, Patrick J Kennedy, and T Tse William. Bistable switches control memory and plasticity in cellular differentiation. *Proceedings of the National Academy of Sciences*, 106(16):6638–6643, 2009.

- [60] Shian-Jang Yan, Jeremiah J Zartman, Minjie Zhang, Anthony Scott, Stanislav Y Shvartsman, and Willis X Li. Bistability coordinates activation of the egfr and dpp pathways in drosophila vein differentiation. *Molecular systems biology*, 5(1):278, 2009.
- [61] H. Yu, B. L. Moss, S. S. Jang, M. Prigge, E. Klavins, J. L. Nemhauser, and M. Estelle. Mutations in the tir1 auxin receptor that increase affinity for auxin/indole-3-acetic acid proteins result in auxin hypersensitivity. *Plant physiology*, 162(1):295–303, 2013.

Appendix A

PLASMIDS AND YEAST STRAINS

Plasmid Name	Description	Sequence Link
pMODKan-HO-pACT1-ZEV4	β -e inducible transcription activator ZEV4 driven by a yeast pACT1 promoter. Integrable into yeast HO locus with Kanamycin (Kan) resistance	https://benchling.com/s/i1bMGuVS
pMODT4-pGALZ4-Z4AVNY	Fluorescent, auxin degradable transcription activator Z4AVNY driven by pGALZ4 promoter. Integrable into yeast TRP locus.	https://benchling.com/s/XlO1WLN2
pMODH8-pGPD-TIR1_DM	TIR1_DM driven by yeast GPD promoter. Integrable into yeast HIS locus	https://benchling.com/s/jrSY0pv4
pGPU6-pGALZ4-eYFP	Enhanced YFP driven by pGALZ4 promoter. Integrable into yeast URA locus.	https://benchling.com/s/92oqk1LL
pMODU6-pGALZ4-BleoMX	BleoMX driven by pGALZ4 promoter. Integrable into yeast URA locus.	https://benchling.com/s/WhWPdZTT

Table A.1: Plasmids with descriptions and publicly accessible Benchling links. The specific Zinc finger binding domain used in the bistable switch, ReARM and related circuits is coded as Z4 (short as Z in main text). The pGALZ4 and Z4AVNY refer to pGALZ and ZAVNY in the main text respectively.

Yeast Strain Name	Description	Integrated Plasmids
bistable switch	The bistable switch strain that contains positive feedback loop on fluorescent Z4AVNY transcription factor, constitutively expressed TIR1_DM and ZEV4.	pMODT4-pGALZ4-Z4AVNY pMOD8G-TIR1_DM pMODKan-HO-pACT1-ZEV4
without positive feedback	The strain that does not contain positive feedback on the fluorescent protein eYFP.	pGP6-pGALZ4-eYFP pMOD8G-TIR1_DM pMODKan-HO-pACT1-ZEV4
without auxin receptor	The strain that does not have constitutively expressed auxin receptor comparing to bistable switch strain.	pMODT4-pGALZ4-Z4AVNY pMODKan-HO-pACT1-ZEV4
ReARM	The strain that added pGALZ4 driven BleoMX component comparing to the bistable switch	pMODU6-pGALZ4-BleoMX pMOD8G-TIR1_DM pMODT4-pGALZ4-Z4AVNY pMODKan-HO-pACT1-ZEV4
without bistable switch	The strain that has a β -e inducible BleoMX activated through pGALZ4 promoter by ZEV4.	pMODU6-pGALZ4-BleoMX pMODKan-HO-pACT1-ZEV4

Table A.2: Yeast strains with descriptions along with the plasmids integrated into their genome.